Investigating cellular redox modulation upon Influenza A virus infection

A Thesis

submitted in partial fulfilment of the requirements for the BS-MS Dual Degree Programme at

Indian Institute of Science Education and Research Pune

Dr. Homi Bhabha Road,

Pashan, Pune 411008, INDIA.

by

Khushboo Jain

Department of Biology, IISER Pune

Supervisor: Dr. Shashank Tripathi,

Department of Microbiology and Cell Biology,

Indian Institute of Science, Bangalore

May 2022 to March 2023

Certificate

This is to certify that this dissertation entitled “Investigating cellular redox modulation upon Influenza A virus infection“ towards the partial fulfilment of the BS-MS dual degree programme at the Indian Institute of Science Education and Research, Pune represents study/work carried out by Khushboo Jain at Indian Institute of Science, Bangalore under the supervision of Dr. Shashank Tripathi, Centre for Infectious Disease Research, Department of Microbiology and Cell Biology, IISc Bangalore, during the academic year 2022-2023.

Dr. Shashank Tripathi

Committee:

Dr. Shashank Tripathi

Dr. Satyajit Rath

This thesis is dedicated to my parents, Dr. Preeti Jain
and Dr. Manish Jain.

Declaration

I hereby declare that the matter embodied in the report entitled “Investigating cellular redox modulation upon Influenza A virus infection“ are the results of the work carried out by me at the Department of Microbiology and Cell Biology, Indian Institute of Science, Bangalore, under the supervision of Dr. Shashank Tripathi, and the same has not been submitted elsewhere for any other degree.

Khushboo Jain

Date: 10th April, 2023

Table of Contents

List of Tables

List of Figures

Abstract

The Influenza A virus (IAV) is a dangerous respiratory pathogen that infects millions of people worldwide every year, causing significant morbidity and mortality. Although IAV is a well-known virus, much remains unknown about the molecular mechanisms underlying its pathogenesis. One of the key aspects of IAV pathophysiology is its interference with redox homeostasis within cells. IAV causes acute infections leading to a sharp increase in oxidative stress at later stages of infection. However, only few studies attempt to decipher the molecular processes of Influenza A virus-induced redox perturbation. We exploited a genetically encoded redox biosensor to measure cellular redox potential following IAV infection with high sensitivity and temporal resolution. We explored the cell-type differences and IAV strain-to-strain differences in redox regulation, and sought to identify the viral proteins responsible for this regulation. Altogether, our research underscores the importance of careful investigation of the relationship between IAV pathogenesis and redox modulation, with a focus on viral components involved, to aid in the development of effective antiviral therapeutic avenues.

Acknowledgments

I would like to express my sincere gratitude to my supervisor, Dr. Shashank Tripathi, for his unwavering support and guidance throughout my project. I would also like to thank him for providing me with all the necessary resources to carry out my research work.

I would also like to extend my heartfelt thanks to all the members of ST Lab. Their support, encouragement, and constructive feedback have helped me broaden my knowledge and improve my research work. I have learned so much from our discussions, and I am grateful for the friendships that have developed during my time in the lab. I would specially like to thank Oyahida Khatun for her mentorship and Mansi Sharma for her input on the techniques used.

Lastly, I would like to thank my parents for being a constant source of support and motivation. I would also like to thank my friends Aishwarya Juneja and Goirik Chakrabarty for being supportive and encouraging throughout my research journey.

Contributions

Contributor name	Contributor role
Dr. Shashank Tripathi, Oyahida Khatun, Khushboo Jain	Conceptualization Ideas
Khushboo Jain, Oyahida Khatun, Mansi Sharma	Methodology
Mansi Sharma, Khushboo Jain	Software
Dr. Shashank Tripathi	Validation
Khushboo Jain, Mansi Sharma	Formal analysis
Khushboo Jain	Investigation
Dr. Shashank Tripathi	Resources
Khushboo Jain	Data Curation
Khushboo Jain	Writing - original draft preparation
Khushboo Jain, Dr. Shashank Tripathi	Writing - review and editing
Khushboo Jain, Oyahida Khatun, Dr. Shashank Tripathi	Visualization
Dr. Shashank Tripathi	Supervision
Dr. Shashank Tripathi	Project administration
Dr. Shashank Tripathi	Funding acquisition

This contributor syntax is based on the Journal of Cell Science CRediT Taxonomy[1].

[1] https://journals.biologists.com/jcs/pages/author-contributions

1. Introduction

Influenza A viruses are enveloped viruses that continuously change in several animal hosts, including humans (Taubenberger and Kash, 2010). Human Influenza A viruses (IAV) are a serious concern for public health and global economy, having caused pandemics and seasonal epidemics. The Spanish flu of 1918 (H1N1), the Asian flu of 1957 (H2N2), the Hong Kong flu of 1968 (H3N2), the bird flu of 2003 (H5N1) and 2013 (H7N9), and the swine flu of 2009 (H1N1) are some notable examples of IAV pandemics (Past Pandemics | Pandemic Influenza (Flu) | CDC, 2019). Compared to annual and epidemic IAV outbreaks, pandemic IAVs are associated with more significant morbidity and mortality. IAV infection affects both upper and lower respiratory tracts, and it might cause pneumonia, which is promoted by subsequent bacterial infections in some cases. At least 50 million people died as a result of the 1918 IAV pandemic, which is regarded as the deadliest pandemic in history (Taubenberger and Morens, 2006). Vaccination is currently the main strategy to prevent IAV infections, but its effectiveness is constrained by our inability to create vaccines that specifically target newly discovered IAV strains. IAV infections continue to be a hazard, therefore it is critical to design new countermeasures against them quickly and to deepen our understanding of their biology.

1.1 Influenza virus and virus life cycle

Influenza A is an enveloped virus belonging to the *Orthomyxoviridae* family (Krammer *et al.*, 2018). The IAV genome consists of eight single-stranded, negative-sense viral RNA (vRNA) segments (HA, NA, NP, M, PA, PB1, PB2 and NS) that typically encode 11 or 12 viral proteins (Bouvier and Palese, 2008). Viral RNA segments bind to viral polymerase and are surrounded by several copies of nucleoprotein to form viral ribonucleoprotein (RNP) complexes (Eisfeld *et al.*, 2015). On the basis of the antigenic properties of hemagglutinin (HA) and neuraminidase (NA) surface glycoproteins, IAVs are categorized into eighteen HA subtypes (H1–H18) and eleven NA subtypes (N1–N11) (Russell, 2016). Gene mixing, gene reassortment, and antigenic drift lead to the emergence of novel strains capable of causing pandemics.

The IAV envelope is composed of a lipid bilayer which includes the hemagglutinin (HA), neuraminidase (NA), and matrix 2 (M2) transmembrane proteins (Samji, 2009). The virus life cycle involves several steps – virus attaches to the target cell and enters, viral ribonucleoproteins are uncoated and released into the nucleus for replication and transcription of viral RNA, and subsequently viral components assemble and virus budding takes place (Samji, 2009). HA, a homotrimer, which is the main surface glycoprotein on the viral lipid membrane, functions both as the virus receptor binding and fusion protein (Samji, 2009). HA binds to the sialic acid exposed on the host cell surface (Krammer *et al.*, 2018). Cleavage of HA via host cellular proteases, into HA1 and HA2 subunits, facilitates the fusion of viral envelope and the cellular endosomal membrane (Dou *et al.*, 2018). The subunits are linked through disulphide bonds (Huang *et al.*, 2003). Virus is internalized through receptor-mediated endocytosis and it enters an endosome within the cell. The low pH of the endosome stimulates the viral and endosomal membranes to fuse, which causes the M2 ion channel to open and the viral ribonucleoprotein (vRNP) is released from M1 (Pinto and Lamb, 2006).

After being released in the host cell cytoplasm, vRNPs need to reach inside the nucleus for influenza viral transcription and replication. Viral polymerases (PA, PB1, PB2) and nucleoprotein (NP) form the vRNP, and they each have a nuclear localization signal (NLS), which interacts with the nuclear import machinery to facilitate their entry into the nucleus. The vRNP import into the nucleus takes place through the importin α and β dependent nuclear import pathway (Eisfeld *et al.*, 2015; Dou *et al.*, 2018). In the nucleus, vRNPs are transcribed and replicated with the help of viral RNA polymerase complexes. The viral RNA polymerase complexes consist of three polymerase (3P) proteins: PA, PB1, and PB2. PB1 and PB2 proteins bind to the vRNP, and PA serves as a bridge between them (Nayak *et al.*, 2009). The 3P complex executes the transcription and replication of viral genes within nucleus. The vRNPs generated are exported out from nucleus through the nuclear pore complex, which is aided by the nuclear export protein (NEP) (Boulo *et al.*, 2007). After assembly and packaging with other viral proteins, the virions bud through the host cell plasma membrane, producing new infectious influenza viruses. The budding process is driven via the viral matrix protein (M1),

which interacts with the cytoplasmic domains of HA and NA to promote their incorporation into the viral envelope (Baudin *et al.*, 2001; Nayak *et al.*, 2009).

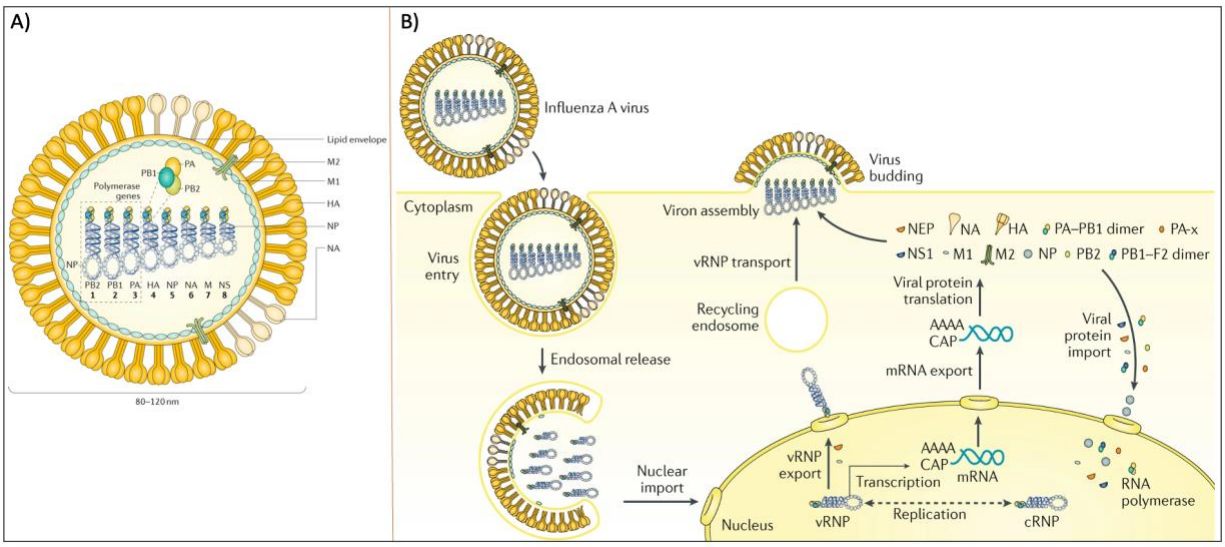

Figure 1. Overview of the Influenza A virus. Influenza virion is shown in panel (A) and virus life cycle is shown in panel (B). (Adapted from *Nat Rev Dis Primers. 2018*)

The strains of IAVs, such as H1N1, H3N2, and H5N1, differ in their antigenic properties, structure, and pathogenicity. H1N1 virus has a hemagglutinin (HA) subtype that mainly recognizes the sialic acid (SA)-α-2,6-Gal-terminated saccharides found in humans, as opposed to the hemagglutinin of avian H5N1 viruses, which primarily bind to SA-α-2,3-Gal-terminated saccharides (Krammer *et al.*, 2018). H3N2 viruses have evolved to undergo more frequent antigenic drift and lead to numerous seasonal epidemics (Allen and Ross, 2018). H5N1, interestingly, has a unique feature called a polybasic cleavage site in the HA protein, facilitating its systemic replication and dissemination, leading to increased pathogenicity and mortality (Bogs *et al.*, 2010).

1.2 Redox biology in cells

To maintain reduction-oxidation (redox) balance, cells produce and remove reactive oxygen and nitrogen species (ROS and RNS, respectively) (Mp, 2009). The redox status gets altered during several cellular processes like signaling, differentiation, proliferation, and metabolism. Oxidative stress, persistent immune response activation, and inflammation can occur when the cells are

unable to remove ROS/RNS, or their scavenging systems deplete (Mittal *et al.*, 2014).

ROS are short-lived oxygen intermediates, some examples being the superoxide anion (O_2•−), hydroxyl radical (HO•), and hydrogen peroxide (H_2O_2) (Mp, 2009). These are formed as by-products through enzymatic and non-enzymatic redox changes in mitochondria, plasma membrane, peroxisomes, and cytoplasm in the cell (Schrader and Fahimi, 2004; Di Meo *et al.*, 2016). The main intracellular ROS generators are nicotine adenine dinucleotide phosphate (NADPH) oxidase (NOX) enzymes, xanthine oxidase, and cytochrome P450 (Gottlieb, 2003; Bedard and Krause, 2007). Reactive nitrogen species (RNS) consist of nitric oxide (•NO), peroxynitrite (ONOO−) and nitrogen dioxide ($•NO_2$) (Di Meo *et al.*, 2016). ROS/RNS damage proteins, lipids, DNA, and mitochondria, causing cellular dysfunction (Kaushal *et al.*, 2019).

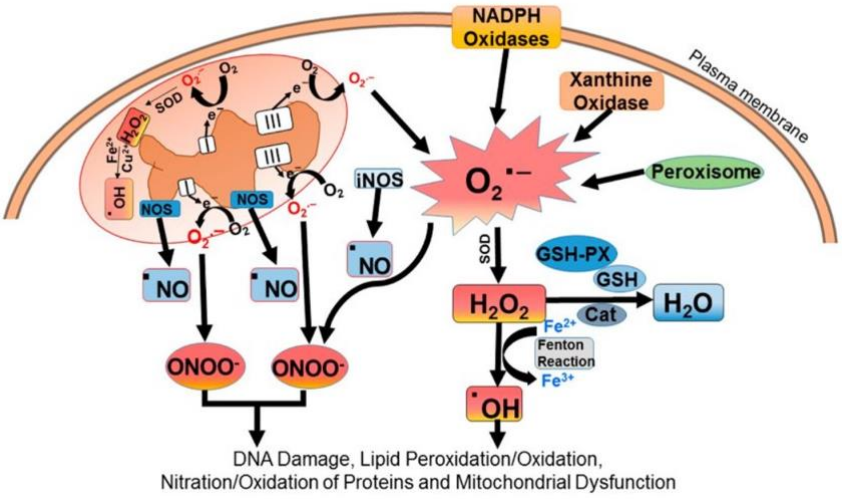

Figure 2. Redox biology in cells. The figure represents cellular sources, pathways and downstream effects of reactive oxygen species and reactive nitrogen species. (Adapted from *Int. J. Mol. Sci. 2019*)

Cells regulate the redox status under physiological conditions through enzymatic as well as non-enzymatic antioxidant systems. Some examples of antioxidant enzymes are - superoxide dismutases (SOD), catalases (CAT), glutathione peroxidase (GPx), peroxiredoxins (Prdx) and glutaredoxins (GRs) (Chen *et al.*, 2020). The cytosolic SOD and mitochondrial MnSOD convert superoxide O_2•− to hydrogen peroxide (H_2O_2), which metal ions like Fe and Cu catalyze to form hydroxyl radicals (OH•)

(Fukai and Ushio-Fukai, 2011). Hydrogen peroxide is removed by catalase and glutathione-peroxidase (GPx), being reduced to H_2O (Schrader and Fahimi, 2004).

The non-enzymatic antioxidants include molecules like glutathione (GSH), which is a major cellular antioxidant, and flavonoids, carotenoids, melatonin, vitamin C and E (Chen *et al.*, 2020). The reduced (thiol)/oxidized (disulphide) glutathione couple, GSH/GSSG, depicts the cellular antioxidant index and serves as a redox buffer in cells (R *et al.*, 2005). GSH shields intracellular components from reactive oxygen species, including the free radicals, lipid peroxides, and heavy metals. Additionally, in several RNA viral infections, including influenza viruses, GSH acts as a key player in reducing oxidative stress.

Viruses have evolved to take advantage of cellular redox status to promote their own replication and survival (Khomich *et al.*, 2018). Therefore, understanding the redox biology in cells and how viruses manipulate the redox state is crucial. For example, Hepatitis C virus (HCV) infection is linked to elevated oxidative stress, increased TGF-β and hepatic fibrosis due to higher ROS levels produced by the virus (Boudreau *et al.*, 2009).

1.3 Influenza virus infection and redox perturbations

Similar to other viruses, Influenza employs multiple tactics to manipulate host cell machinery to its benefit. One of these strategies involves disturbing the intracellular redox state, by modulating the activity of various signaling cascades. Microbial infections, ligand and receptor binding, cytokines, and other factors can cause a mild oxidative imbalance. This imbalance can lead to the oxidation of cysteine residues in redox-sensitive proteins in the vicinity of ROS, functioning as a trigger to activate or deactivate protein function in a reversible manner. ROS accumulation after viral infection can also activate innate antiviral immunity. However, some studies suggest that ROS generation favours viruses.

NADPH oxidases (NOXs) are membrane bound enzyme complexes and enable the production of high amounts of ROS upon microbial infections (Abo *et al.*, 1991). Activated NOX generates ROS via a transfer of electrons to O_2 to release

$O_2^{\bullet-}$ on the other side of the cell membrane (Yang *et al.*, 2011). Induced NOX4 was demonstrated as a major ROS generator in cells infected with Influenza A virus (Amatore *et al.*, 2015). NOX4 activation was suggested to activate cellular signaling pathways including the mitogen-activated protein kinase (MAPK) pathways such as p38 and JNK (Jaulmes *et al.*, 2009; Wu *et al.*, 2010). The p38 MAPK and JNK are involved in the inflammatory and apoptotic responses to the infection, and might promote nuclear export of viral ribonucleoproteins (Amatore *et al.*, 2015). Therefore, NOX4 activation might regulate certain steps of virus replication-cycle. On the other hand, NOX2, which is another ROS-generating enzyme, was reported to be downregulated by IAV infection (Amatore *et al.*, 2015). NOX2 mediates host antiviral response for other viral infections, therefore NOX2 reduction by influenza virus could be an immune evasion strategy (Amatore *et al.*, 2015). Additionally, a reduction in the expression of nuclear factor erythroid 2-related factor 2 (NRF2), which is a major cellular antioxidant enzyme, was associated with IAV infection (De Angelis *et al.*, 2022).

Superoxide dismutase (SOD1) overexpression was shown to reduce intracellular levels of IAV polymerase PB1 (Pyo *et al.*, 2014). H5N1 infection in lung epithelial A549 cells induced decrease in SOD1 expression levels according to a study (Lin *et al.*, 2016). Importantly, several studies have suggested that Influenza virus replication heavily relies on the depletion of reduced glutathione (GSH) (Khomich *et al.*, 2018; Chen *et al.*, 2020). Exogenous supplementation with GSH inhibited replication of IAV, whereas GSH depletion by buthionine sulfoximine (BSO) ultimately increased viral titres (Ciriolo *et al.*, 1997).

GSH is suggested to inhibit the formation of IAV matrix proteins, IAV replication, and generation of virus progeny (Cai *et al.*, 2003). Influenza virus disturbs the redox homeostasis mediated by GSH, which then promotes the formation of more virus particles, and leads to cell death (Cai *et al.*, 2003). The process and players involved in this GSH downregulation, however, are still not known.

Interestingly, some studies have reported a biphasic modulation in the generation of ROS as a viral tactic to take advantage of the redox cell response. Several kinases which get activated upon IAV infection, like the MAP kinases and the PKC family, are redox-sensitive (Truong and Carroll, 2013). In particular, the addition of exogenous

H_2O_2 induces production of H_2O_2 and activates the MAPKs (Truong and Carroll, 2013). Upon IAV infection, a study showed evidence of a biphasic activity wherein MAPK activation was increased during viral entry stage, as well as during late stages when nuclear export of viral nucleoprotein (NP) takes place, with a reduction in between (Foo *et al.*, 2022). Since MAPK is known to be activated by ROS, it is conceivable that Influenza virus dynamically modifies the redox balance of host cells during the course of its infection.

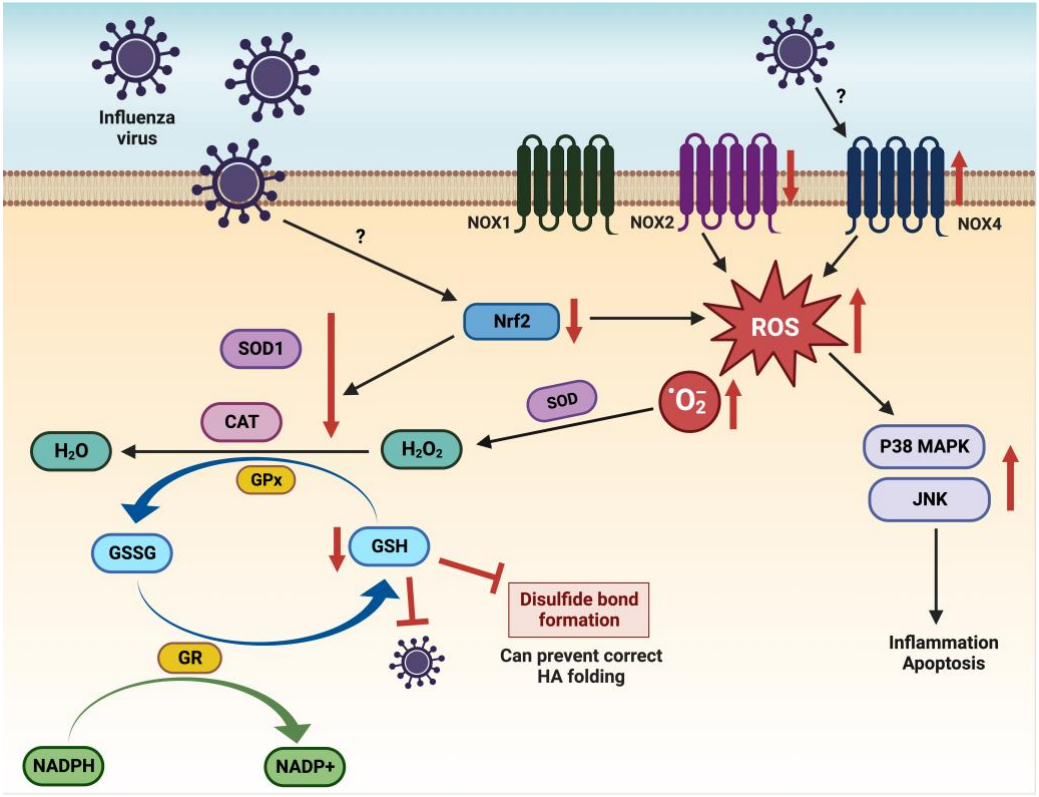

Figure 3. Redox-related pathways affected by Influenza A virus. The schematic depicts an upregulation (red, up arrow), downregulation (red, down arrow) of cellular factors and pathways, or inhibition of processes, caused after Influenza virus infection. Illustrated with Biorender.com.

1.3.1 Influenza viral proteins and redox states

Cellular glycoprotein folding occurs in the endoplasmic reticulum, which is regulated by the oxidative environment and activity of oxidoreductases like protein disulphide isomerase (PDI) (Ellgaard and Ruddock, 2005; Zeeshan *et al.*, 2016). Influenza virus

hijacks the host's secretory pathway to produce its own glycoproteins, and redox-regulated PDI chaperones play a crucial function in the formation of disulphide bonds between cysteines in viral hemagglutinin (HA) protein, which is an oxidative process and is necessary for its maturation (Chamberlain *et al.*, 2019). Thus, the process could strongly be disturbed by reducing agents such as glutathione (GSH) and the reduction in GSH levels upon infection can be a strategy to favour HA folding (Sgarbanti *et al.*, 2011). Sgarbanti *et al.* reported that GSH-C4 (a glutathione analog) led to a retention of HA in the endoplasmic reticulum, where it remained a monomer with incomplete folding. Nonetheless, the molecular mechanism governing this outcome has not been thoroughly investigated.

A study implicated that PB1-F2 protein, which localizes in the mitochondria, is involved in ROS production in lung epithelial A549 cells (Shin *et al.*, 2015). The researchers observed that PB1-F2 overexpression led to a downregulation of SOD1, which is a major cellular antioxidant enzyme. In addition, a study reported that M2, a proton channel protein, could increase the production of ROS after transfection in A549 cells (Lazrak *et al.*, 2009). They suggested that M2 elevated the steady state ROS levels and thus activated protein kinase C (PKC). However, the study utilized a redox sensing dye for ROS detection, which is prone to show non-specificity (Rota *et al.*, 1999). A study suggested that single protein expression of hemagglutinin, matrix protein, and nucleoprotein could serve as an activator of NFκB through oxidative radical production and IκB kinase (IKKβ) activation (Flory *et al.*, 2000).

However, not many studies have looked into the molecular processes involved in Influenza A virus mediated modulation of ROS, and even lesser have investigated the viral proteins responsible for this modulation. Further investigation is required to understand the regulation of the redox environment by viral components during different stages of viral life cycle. Identifying viral targets will aid the development of antiviral therapeutics.

To gain insight, it is necessary to measure redox changes with high spatiotemporal resolution and specificity for cellular redox pairs without disrupting cellular function. It is yet unclear whether redox changes observed in previous studies were due to infected cells, bystander uninfected cells, or both. Answering these questions can help identify redox-modulating drugs to treat or prevent viral infections.

1.4 Redox reporter system

Redox-sensitive dyes like 2′,7′-dichlorodihydrofluorescein diacetate (DCFDA) are commonly used to detect redox status, but they have inherent limitations, including non-specificity and the ability to interact with multiple oxidants like metals, peroxidases, cytochrome *c*, and become oxidized without the presence of ROS (Zuo and Clanton, 2002; Tarpey *et al.*, 2004). Furthermore, they may promote artificial ROS formation (Rota *et al.*, 1999). Conventional methods to study redox are also invasive and disrupt cellular integrity. Measuring cellular redox states accurately is challenging due to these limitations.

To overcome the limitations, genetically encoded redox sensors via the modification of green fluorescent protein (GFP) have been developed (Albrecht *et al.*, 2014). These sensors, for instance a reduction-oxidation sensitive green fluorescent protein (roGFP), can be directed to subcellular compartments, allowing for quantitative and dynamic redox related observations (Meyer and Dick, 2010).

The roGFP2 is designed by the mutating two amino acids of the enhanced GFP to cysteines (S147C, Q204C) allowing a formation of disulphide bond between the cysteines during favourable oxidative environments (Lohman and Remington, 2008). The oxidation of cysteines forms a disulphide bond, leading to an increase in the fluorescence intensity at 400 nm and relative decrease at 490 nm. Owing to the reversible disulphide formation, there is a shift in the protonation condition of the chromophore due to structural changes (Dooley *et al.*, 2004; Hanson *et al.*, 2004). The disulphide bond formation causes a conformational change that moves Tyr66 further from the chromophore, leading to a shift in the chromophore excitation spectra (Hanson *et al.*, 2004). The biosensor can detect long-term as well as short-term modulations of the redox potential.

The roGFP2 biosensor was further linked with human glutaredoxin-1 (Grx1) in order to facilitate precise real-time equilibration between the glutathione redox couple and redox reporting pair ($roGFP2_{red}$ and $roGFP2_{ox}$) (Gutscher *et al.*, 2008). This composite biosensor, called Grx1-roGFP2, has improved sensing properties that increase the specificity of roGFP2 for GSH/GSSG couple, which abolished the

biosensor's reliance on endogenous Grx. The ratio of GSH and GSSG levels is known to provide dynamic indication of oxidative stress *in vivo* (Jones, 2002). Having Grx1 and roGFP2 nearby in the sensor drives quick equilibration amongst the dithiol-disulphide of glutathione and roGFP2 (Gutscher *et al.*, 2008). The redox sensor thus facilitates precise imaging and measurements of glutathione redox potential (E_{GSH}) temporally and in different cellular compartments (Morgan *et al.*, 2011).

The ratio of emitted fluorescence at two fluorescence excitation maxima (around 400 and 490 nm) give the redox sensor readout. Due to a ratiometric response, the redox biosensor readout reduces or eliminates data anomalies due to photobleaching, illumination stability, excitation path length, and nonuniform indicator distribution across cells and cell populations.

With the application of this sensor can help decode the cellular redox variation upon Influenza A virus infection. By investigating the effects of altering redox states on viral infection and replication, spatially and temporally, we can gain a better understanding of redox modulation caused by viral infection and replication. This redox reporting strategy can later be implemented *in vivo* in animal models to further shed light on the understanding of redox modulation caused by viral infection and replication.

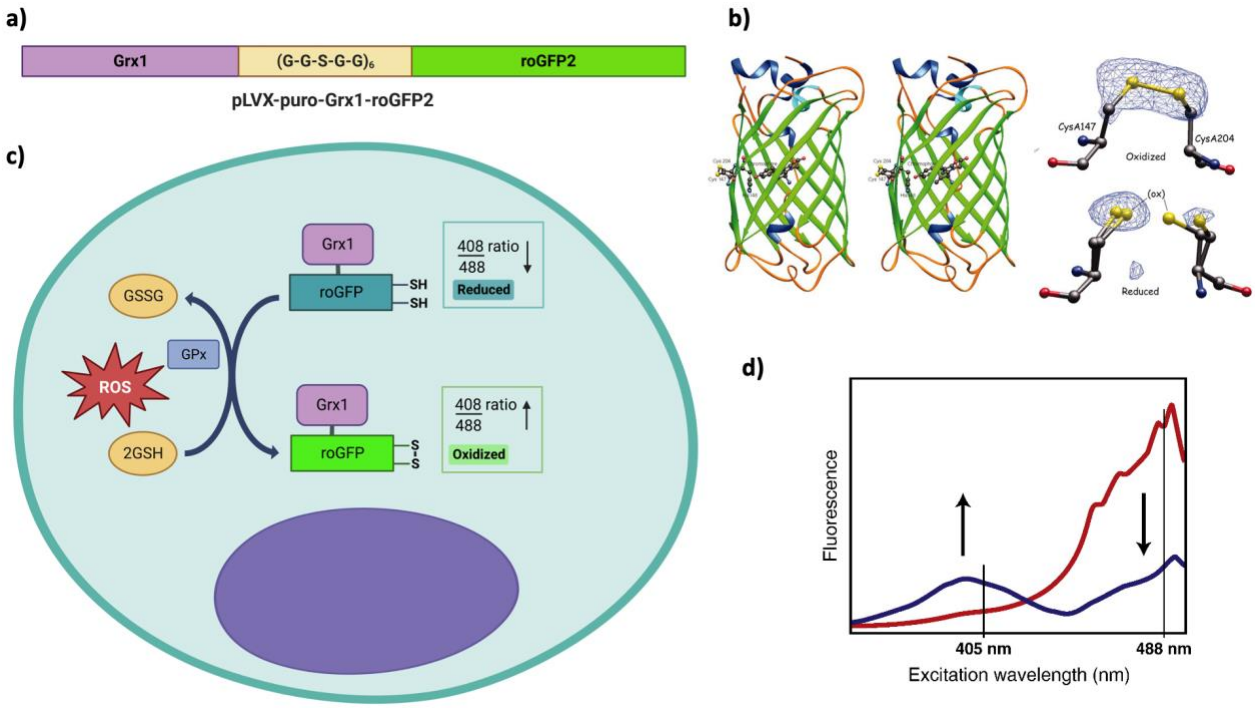

Figure 4. Redox reporting biosensor. Panel (a) shows the pLVX-Grx1-linker-roGFP2 construct utilized in the study as a redox biosensor. Panel (b) represents the structure of reducing-oxidizing sensitive GFP (roGFP2) and formation of a disulphide bond between mutated cysteines in oxidized form (disulphide), versus breakage in bond in the reduced form (thiol) (adapted from *J Biol Chem. 2004*). Panel (c) is a illustration demonstrating Grx1-roGFP2 oxidation and reduction in the presence of ROS in cell. GPx denotes the glutathione peroxidase in cells. Panel (d) depicts the fluorescence excitation spectra of roGFP2 for completely reduced (red line) or completely oxidized (blue line) versions, with an emission at 510 nm (adapted from *Free Radic Biol Med. 2011*).

1.5 Aim and Objectives

Aim - To study Influenza A virus-mediated redox modulation within cells. Further, to find any Influenza viral component involved in redox perturbation post infection, in order to formulate potential antiviral strategies.

Objectives -

1. Generate Grx1-roGFP2 redox biosensor expressing stable cell lines.
2. Investigate temporal redox changes in stable cells upon infection with different strains of Influenza A virus (IAV).
3. Screen IAV proteins for their involvement in observed redox modulations.
4. Distinguish the redox status of IAV infected versus uninfected bystander cells.

2. Materials and Methods

2.1. DNA Transformation

The competent cells (Stbl3 E.coli) were used for transformation and propagation of various DNA constructs. For transformation, about 100 ng of DNA was added into 50 µl of competent cells in 1.5 ml microfuge tubes and incubated on ice for 30 min. For heat shock, the tubes were transferred to a 42°C water bath for 90 seconds followed by 10 minutes incubation on ice. 450 ml LB media was added to the cells and incubated at 37°C with shaking for 1 hour. The cells were then pelleted down, 350 µl supernatant was discarded and cells were resuspended in remaining 150 µl of LB medium and plated on LB agar plates containing the

appropriate antibiotic. Plates were kept for 12-16 hours at 37°C for the appearance of colonies.

2.2. Plasmid DNA Isolation

DNA minipreps were carried out by isolating plasmid DNA from 5 ml bacterial cultures grown overnight, using the G Biosciences kit (catalog no. 786-361-300P), as per the manufacturer's instructions. The concentration and quality of eluted plasmid DNA was checked using a NanoDrop spectrophotometer instrument and the plasmids were then stored at -20°C.

2.3. Cell culture

Human lung adenocarcinoma (A549), Human Embryonic Kidney (HEK293T) and Madin-Darby Canine Kidney (MDCK) cell lines were cultured in Dulbecco's modified Eagle's Medium (DMEM) supplemented with 10% fetal bovine serum (FBS) and 1X penicillin-streptomycin glutamine, and were sub-cultured on reaching 90% confluency. All cell lines were cultured at 37°C in a 5% CO_2 incubator.

2.4. Grx1-roGFP2 biosensor expression construct

The Grx1-roGFP2-containing vector was constructed by Dr. Tobias P. Dick's lab (Gutscher *et al.*, 2008). The construct consists of human Grx1 fused to the N terminal of roGFP2, with a linker in between. The linker is a 30 amino acid sequence, $(Glycine\text{-}Glycine\text{-}Serine\text{-}Glycine\text{-}Glycine)_6$ to provide flexibility between the linked Grx1 and roGFP2 sequences. The Grx1-roGFP2 sequence was present in a pLVX puro vector backbone. Within cells, Grx1-roGFP2 expressed and localized in the cytoplasm. Thus, the complete construct was pLVX-puro-cyto-Grx1-roGFP2.

Due to a conformational change in the roGFP2 structure, the fluorescence intensity increases at 408 nm excitation upon oxidation, and relatively decreases at 488 nm, although an inverse response is detected upon reduction. The ratio of mean fluorescence intensity upon 408 nm by 488 nm excitation thus increases upon oxidation and decreases upon a reduction in the redox status of cytosolic environment. Therefore, the ratiometric biosensor response was measured and

measurements were independent of changes in cell density, pH and protein content. The covalently fused Grx1 moiety catalyzed the specific equilibration of the roGFP2 dithiol-disulphide redox pair with the glutathione redox pair (GSH/GSSG) in the cell.

2.5. Transfection using Lipofectamine

HEK293T cells were seeded in 6-well (0.5 million cells/well) or 24-well plates (0.1 million cells/well) on the previous day. At about 50% confluency, cells were transfected with DNA using Lipofectamine 2000 (Invitrogen, Carlsbad, CA USA). DNA (500 ng/well for 24 well plate) and lipofectamine (1 µl per 500ng of DNA), in appropriate ratio (usually 1:2 ratio), were added to Opti-MEM in separate vials to make up the volume to 50µl each and incubated for 5 min at room temperature. After 5 min, both DNA + Opti-MEM and lipofectamine + Opti-MEM solutions were mixed and incubated at room temperature for 25 min to allow formation of a DNA-lipid complex. Finally, to each 100 µl of the DNA-lipid mixture was added drop-wise and incubated at 37°C. After 4-6 h of incubation, the medium was removed and fresh complete medium containing DMEM and 10% FBS was added. The cells were harvested for analysis at 36 hours post-transfection, when required.

2.6. Lentivirus preparation

Redox biosensor construct cloned into a lentiviral vector, pLVXpuro-cyto-Grx1-roGFP2, was utilized to prepare lentivirus. This vector along with the helper plasmids (VSVg and Gag-Pol) was used to prepare lentivirus stocks. pLX-GFP lentiviral plasmid was also used to prepare lentivirus simultaneously, to be later used as a transduction control. For this, 0.5 x 10^6 HEK293T cells/well were seeded in a 6-well plate the previous day. Cells were transfected with 2 µg Lentiviral plasmid mix per well of the 6-well plate using 4 µl Lipofectamine 2000 (thus DNA: Lipofectamine in 1:2 ratio). The lentiviral plasmid mix (2 µg) consisted of 1 µg Lentiviral expression plasmid + 0.6 µg Gag-Pol + 0.4 µg VSVg plasmid. The media was changed 6-12 hours later. 48 hours and 72 hours later, the supernatant was collected and pooled. The pooled supernatant was centrifuged at 1200 rpm for 5 min at 4℃ to pellet the debris. The supernatant was then filtered with 0.45 micron syringe filter, and aliquots were stored at -80℃.

2.7. Lentiviral transduction for stable cell line generation

The target cell lines - A549, MDCK and HEK293T, were plated in 6-well plates the previous day. After reaching 70-80% confluency, cells were washed with 1X PBS. Lentiviral transduction media was prepared, containing DMEM supplemented with 8 µg/ml of polybrene as a transducing agent. Then 1 ml of this media was mixed with 1 ml of lentivirus containing supernatant. In each well of the three target cell lines, 1 ml of this lentivirus mix was added, for transduction. Plate was gently swirled and incubated at 37˚C and 5% CO_2. The media was changed to complete media (DMEM + 10% FBS) after 12 hours. After completion of 48 hours since transduction, previous media was discarded and fresh 2 ml of selection media containing Puromycin drug at a concentration of 1 µg/ml was added to the A549 and HEK293T cells, and 10 µg/ml for MDCK transduced cells. pLX-GFP lentivirus was also transduced as a transduction control. After every 48 hours, media was replaced with fresh drug containing selection media, until all non-transduced control cells died, to complete selection of stably transduced cells.

2.8. Flow cytometry of redox sensor expressing cells

The ratiometric response of Grx1-roGFP2 expressing cells was measured by analyzing the ratio of emission (525/40 nm) after excitation at 408 nm and 488 nm on CytoFLEX flow cytometer (Beckman Coulter) instrument. To prepare samples for flow cytometry, the cells adhered to wells of plates were washed with 1X PBS, and detached using trypsin. Trypsin was neutralized with complete DMEM media, and the cell suspension was centrifuged at 3500 rpm for 5 minutes to pellet the cells. The supernatant was discarded and cells were washed with 1X PBS. In case of treatment, after PBS wash, cells were treated with the given concentration of H_2O_2 or DTT for ~3 min before proceeding with flow cytometry analysis.

2.9. Redox Potential Measurements

The intracellular redox potential measurements were conducted as reported in earlier studies (Morgan *et al.*, 2011). For every experiment, the minimal and maximal fluorescence ratios were recorded, corresponding to 100 percent sensor reduction and 100 percent sensor oxidation, using DTT (20 mM) as the reducing agent and H_2O_2 (10 mM) as the oxidizing agent, respectively. The observed

fluorescence ratio was then utilized to calculate the corresponding degree of sensor oxidation using the equation below,

$$OxD_{roGFP2} = \frac{(R - R_{red})}{\frac{I_{488\,min}}{I_{488\,max}}(R_{ox} - R) + (R - R_{red})}$$

where R is the observed ratio; R_{red} and R_{ox} are the ratios of fully reduced and oxidized roGFP2, respectively; $I_{488\ min}$ and $I_{488\ max}$ are the fluorescence intensities measured with excitation at 488 nm for fully oxidized and fully reduced roGFP2, respectively. Next, the intracellular sensor redox potential E_{roGFP2} was calculated, using the modified Nernst equation, mentioned below,

$$E_{roGFP2} = E^{0'}_{roGFP2} - \frac{RT}{2F} ln \frac{(1 - OxD_{roGFP2})}{OxD_{roGFP2}}$$

where roGFP2 has an average consensus midpoint redox potential of $E^{0'}_{roGFP2}$ = −280 mV (Morgan *et al.*, 2011). Given the equilibration between the sensor and the glutathione redox couple, we obtain the glutathione redox potential $E_{GSH} = E_{roGFP2}$.

2.10. Influenza A virus infection

Influenza virus strain H1N1 (PR8) (A/Puerto Rico/8/1934) (virus titre = 8.5 x 10^8 plaque forming units or pfu per ml) was used for infecting mammalian A549 cells and MDCK cells. A549 cells were also infected with the seasonal influenza A virus H3N2 (A/Wisconsin/15/2009) (ATCC VR-1882; titre = 1.3 x 10^9 pfu/ml), and a human isolate of avian influenza H5N1 (HALo) (A/Vietnam/1203/2004) virus (titre = 1.3 x 10^8 pfu/ml). The H5N1 was originally an isolate from a fatal human case that was engineered to allow biosafety level 2+ work through a deletion in the HA polybasic cleavage site. Viral titres were determined by plaque assay using MDCK cells. Cells were infected at selected multiplicity of infection (MOI), where multiplicity of infection suggests the number of virions added per cell during infection.

$$Volume\ of\ virus\ added = \frac{No.of\ cells \times\ MOI}{virus\ titre\ (pfu/ml)}$$

The cells were seeded in 24-well plates (0.1 x 10^6 cells/well) and were infected at ~ 80 % confluency. Prior to infection, number of cells in a well were counted. The cells were washed with 1X PBS. The respective virus at the required MOI was diluted in Opti-MEM. 100 µL of virus inoculum was added per well and the plates were gently rocked every 10 min for 1 hour, at 37°C. After 1 hour, the inoculum was removed and the virus-infected cells were incubated in serum-free minimal essential medium containing 0.3% bovine albumin and tosylsulfonyl phenylalanyl chloromethyl ketone (TPCK)-treated trypsin (0.1ug/ml for A549 and 1ug/ml for MDCK) at 37°C. Cells were incubated and harvested at later specified time points post-infection.

2.11. Western blotting

Western blot analysis was performed to confirm Influenza A virus infection and check virus levels during the time course of infection in A549 cells. Infected or uninfected cells were washed with 1X PBS and lysed in 1X Laemmli buffer at the specified time points. The lysates were heated for 10 min at 95°C and loaded on 10 percent SDS-PAGE. After separation by SDS-PAGE, the proteins were electrophoretically transferred to PVDF membranes (Bio-Rad). Following transfer, membranes were blocked in Tris-buffered Saline with Tween (TBST) containing 5% skimmed milk for 1 hour at room temperature. Membranes were subsequently incubated with primary antibody Anti-Influenza A Virus Nucleoprotein (NP) antibody (mouse monoclonal; ab128193), overnight at 4°C, at 1:1000 dilution. After washing thrice with TBST, the membranes were incubated with horseradish peroxidase (HRP)-conjugated goat anti-mouse secondary antibody, diluted at 1:5000 in TBST containing 5% skimmed milk. Anti-β actin (HRP-conjugated) was used as loading control. The membranes were washed thrice with TBST, and afterward the blots were visualized using the ECL reagents (enhanced chemiluminescence).

2.12. Cloning strategy for inserting RFP gene in Influenza virus

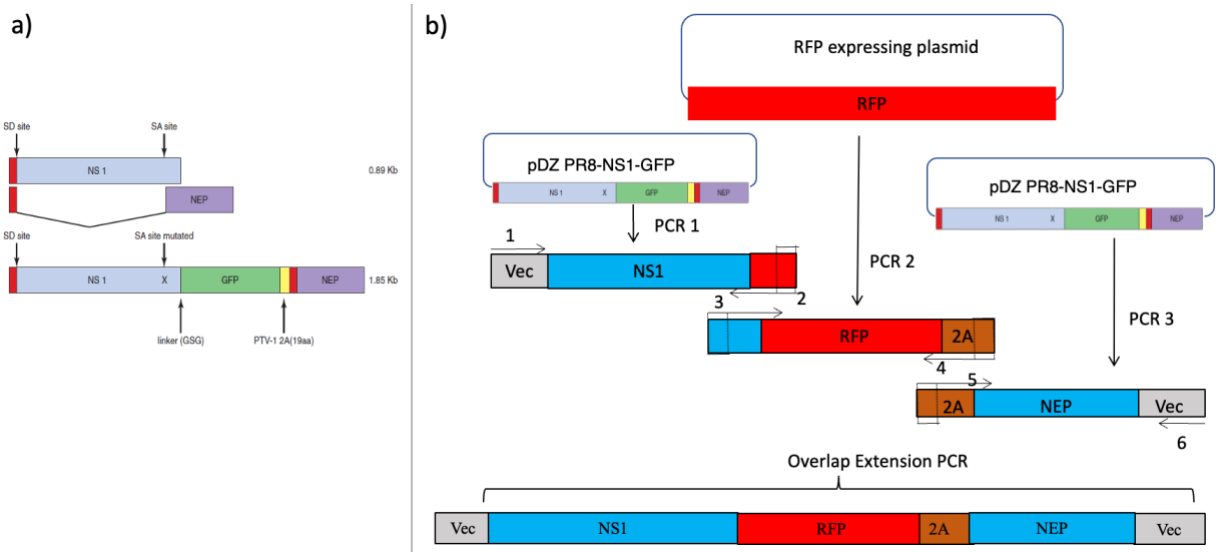

Figure 5. Cloning strategy. (a) Comparison of the NS segment of wild-type and GFP reporter virus. (b) Strategy to insert red fluorescent protein (RFP) gene in viral NS gene segment, to construct NS1-RFP-NEP segment.

To engineer a red fluorescent protein (RFP) expressing Influenza A virus (IAV), the strategy was to insert RFP gene within a viral gene segment, and generate a replication-competent virus with the help of established reverse genetics system (Perez *et al.*, 2013). The smallest viral gene segment, non-structural protein (NS) was modified. The NS segment expresses NS1/NEP proteins by mRNA splicing. To ensure appropriate production of the second protein product - the nuclear export protein (NEP), the splice acceptor site was removed and the NEP open reading frame (ORF) was duplicated and inserted behind a porcine teschovirus-1 2A site, in order to then generate NS1-GFP-NEP construct (Perez *et al.*, 2013). Our strategy was to replace the pre-existing GFP from NS1-GFP-NEP cassette with RFP. For this, NS1, RFP and NEP were amplified. Then overlap extension PCR will allow formation of NS1-RFP and RFP-NEP constructs, which will then be utilized to form the NS1-RFP-NEP cassette (Bryksin and Matsumura, 2010). Primers for overlap extension PCR were designed such that the amplified genes develop complementary overhangs, which act as bridges to help assemble them together. Here, primer 2 & 3 and primer 4 & 5 were complementary to each other.

Genes amplified	Forward primer	Reverse primer	Template
NS1	Primer 1: NS1 Fwd (5' end is pDZ backbone seq with SapI digestion site, 3' end is starting seq of NS1)	Primer 2: NS1-RFP Rev (5' end is starting seq of RFP, 3' end is ending seq of NS1)	pDZ-NS1 WT
RFP	Primer 3: NS1-RFP Fwd (5' end is ending seq of NS1, 3' end is starting seq of RFP)	Primer 4: RFP-2A Rev (5' end is 2A and starting seq of NEP, 3' end is ending seq of RFP)	Rab5 RFP
NEP	Primer 5: RFP-2A Fwd (5' end is ending seq of RFP, 3' end is 2A and starting seq of NEP)	Primer 6: NEP Rev (5' end is pDZ backbone seq with SapI digestion site, 3' end is ending seq of NEP)	pDZ-NS1-GFP-NEP

Table 1: List of primers. The table lists the genes amplified and primers used for cloning.

The sequence of designed primers is mentioned below –

Primer 2: **NS1-RFP Rev**

5'GACGTCCTCGGAGGAGGCCATGCCGCTGCCAACTTCTGACCTAATTGTTC3'

Primer 3: **NS1-RFP Fwd**

5'GAACAATTAGGTCAGAAGTTGGCAGCGGCATGGCCTCCTCCGAGGACGTC3'

Primer 4: **RFP-2A Rev**

5'GTTTCAGCAGGCTAAAGTTGGTCGCGGCGCCGGTGGAGTGGCGGCC3'

Primer 5: **RFP-2A Fwd**

5'GGCCGCCACTCCACCGGCGCCGCGACCAACTTTAGCCTGCTGAAAC3'

After generating the NS1-RFP-NEP cassette, the construct will be digested with SapI enzyme and will be ligated in a pDZ vector backbone digested with same enzyme. Using established reverse genetics strategy, red fluorescent protein expressing replication-competent IAV will be rescued via co-transfection of modified NS1-RFP-NEP plasmid with the remaining rescue plasmids (Perez *et al.*, 2013).

2.13. Statistical analysis

The data represents the mean and the standard deviations (SD). Statistical analysis was performed by GraphPad Prism software version 8.0.2 for Windows (GraphPad Software Inc., San Diego, California, USA).

3. Results

3.1 Flow cytometry analysis of Grx1-roGFP2 expressing cells

We utilized a non-invasive redox biosensor Grx1-roGFP2 (roGFP, reduction-oxidation-sensitive green fluorescent protein), which senses changes in the glutathione (GSH) redox potential, to monitor the dynamic changes in cellular redox physiology. Upon an oxidative stress, the biosensor's fluorescence excitation ratio at 408/488 nm increases, while a reductive stress lead to a decreased ratio. By fitting these ratiometric changes into the equations mentioned earlier, we were able to calculate the E_{GSH} values. However, it is important to note that Grx1-roGFP2 biosensor is limited to measure E_{GSH} between -240 to -320 mV, and fully oxidized or reduced sensor doesn’t necessarily indicate a complete oxidation or reduction of the GSH reservoirs within cells (Gutscher *et al.*, 2008).

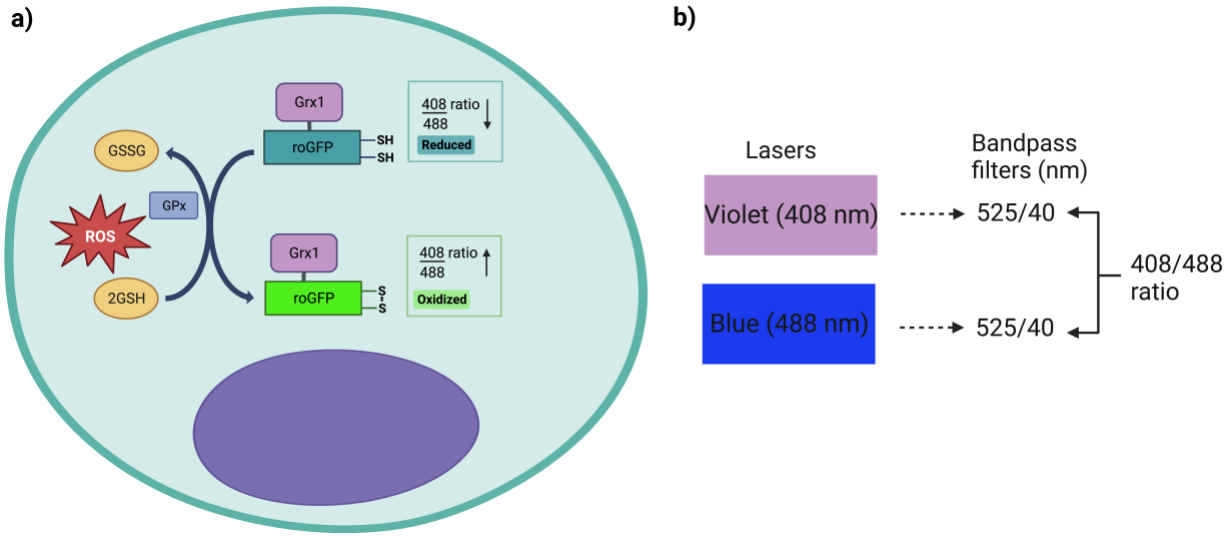

Figure 6. The excitation and emission of redox biosensor in the cell. (a) Schematic of a cell expressing the Grx1-roGFP2 redox biosensor. (b) Representative of the lasers (408 nm and 488 nm) used to excite Grx1-roGFP2 expressing cells, and 525/40 bandpass filters to record emitted fluorescence, in order to take the 408/488 fluorescence ratio.

With the help of flow cytometry, cells expressing the Grx1-roGFP2 biosensor were excited with two wavelengths - 408 nm violet laser and 488 nm blue laser. The emission for both was measured (525/40 nm). The ratio of emission (525/40 nm) after excitation by 408 nm and 488 nm is referred to as the fluorescence ratio (408/488) in the text. Shown below is the gating strategy for (Fig . A) control cells (which did not express the Grx1-roGFP2 redox biosensor). Since these cells were GFP negative, due to the absence of the green fluorescent sensor, a gate was set up for 488 nm excited population (detected by FITC-A channel), to contain only GFP positive cells later (named “roGFP”). Further, only the selected GFP positive population was used for analysis. Control cells were run for each experiment to set the gating. (Fig . B) shows flow cytometry plots for Grx1-roGFP2 expressing A549 cells. The emission upon 488 nm excitation (detected by FITC-A channel) and 408 nm excitation (detected by KO525-A channel) was recorded for the same, GFP positive, population (cells falling within “roGFP” gate). A ratio of mean fluorescence intensity of 408/488 was later calculated as the readout.

A)

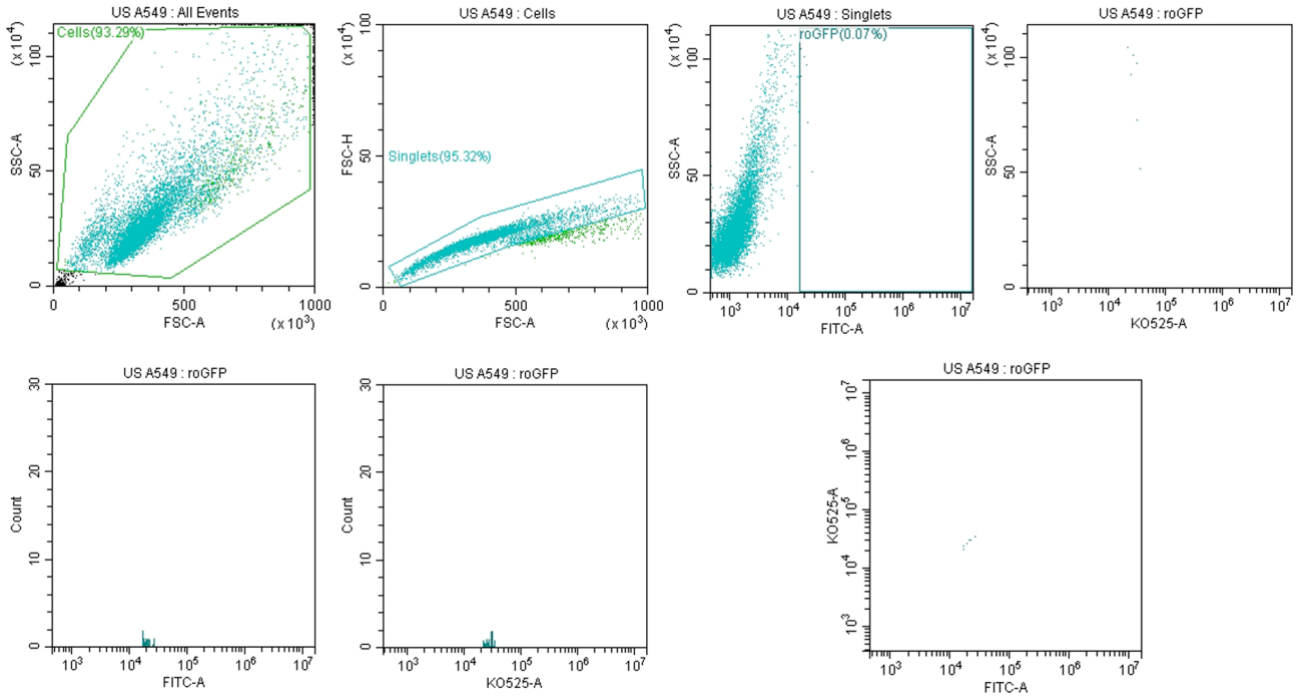

B)

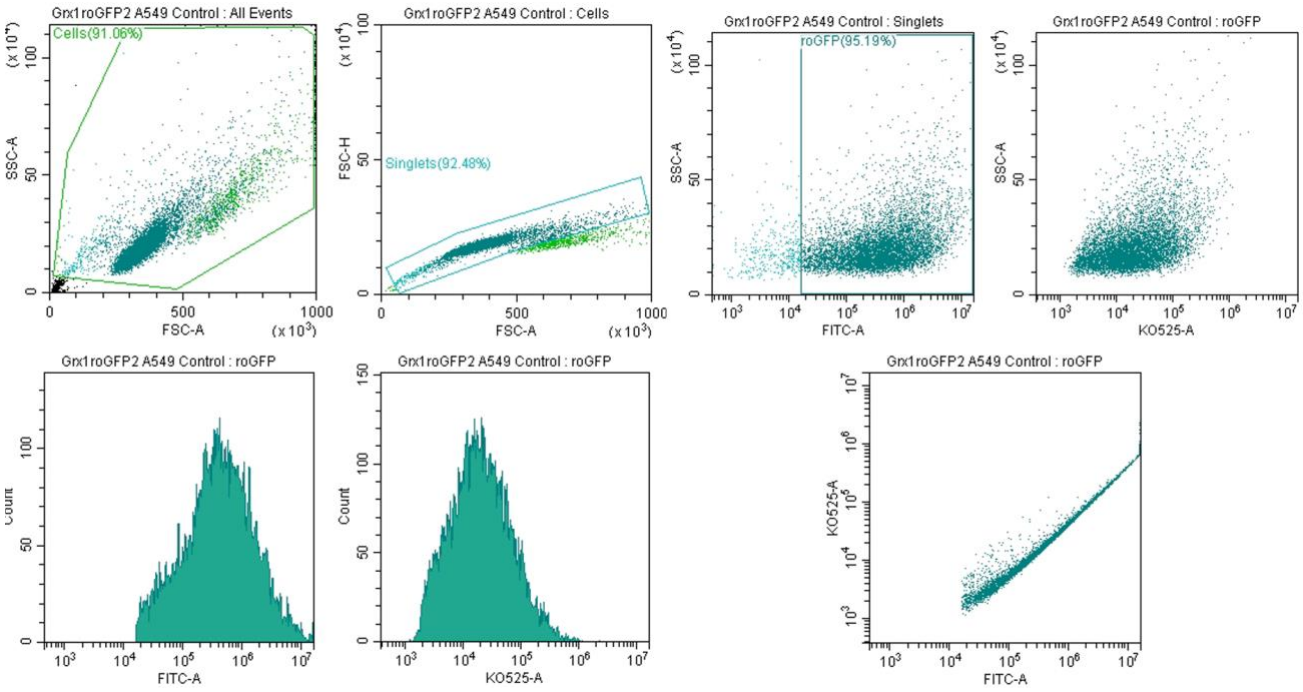

Figure 7. The gating strategy for flow cytometry analysis. (A) Unstained A549 cells were used to set the gating, including the "roGFP" gate to depict GFP positive cells in FITC-A channel. (B) Grx1-roGFP2 expressing A549 cells fell in "roGFP" gate and these selected cells were analyzed further in KO525-A channel.

3.2 Transfection of Grx1-roGFP2 Redox Biosensor

We first tested the activity of the Grx1-roGFP2 redox biosensor, upon transfection in HEK293T cells and A549 cells. We verified the response of the sensor to a well-known cell-permeable oxidant, hydrogen peroxide (H_2O_2), and a cell-permeable thiol reductant, dithiothreitol (DTT). As expected, we could observe that the oxidation of Grx1-roGFP2 in cytosol of HEK293T by H_2O_2 exposure increased the 408/488 ratio, corresponding to E_{GSH} of −240 mV, and reduction with DTT diminished the 408/488 ratio, corresponding to E_{GSH} of −320 mV (Morgan *et al.*, 2011).

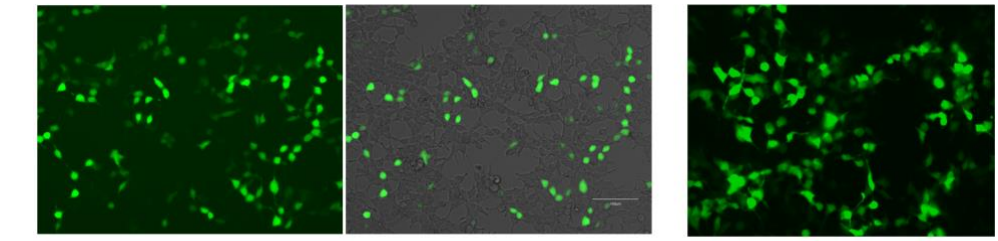

a)

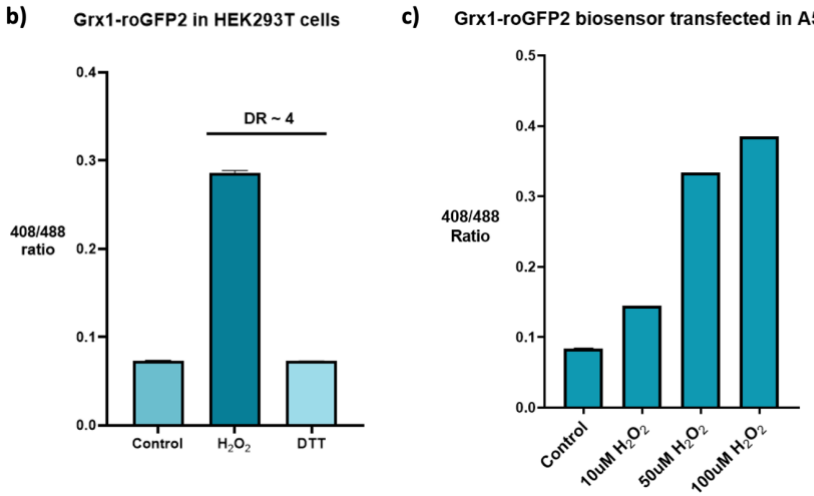

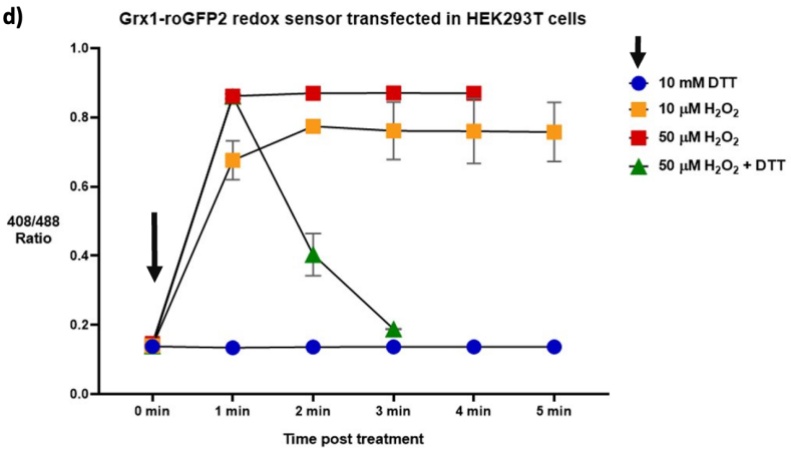

Figure 8. Transfection of Grx1-roGFP2 biosensor in cells. (a) pLVX-Grx1-roGFP2 transfected cells and pLX-GFP (transfection control) transfected cells at 24 hours post transfection. (b) fluorescence ratio changes upon oxidant (H_2O_2) and reductant (DTT) treatment in Grx1-roGFP2 transfected HEK293T cells. DR depicts the dynamic range. (c) fluorescence ratio upon treatment with different oxidant (H_2O_2) concentrations in Grx1-roGFP2 transfected A549 cells. (d) Dynamic changes in fluorescence ratio on adding 10 mM DTT, 10 µM H_2O_2 or 50 µM H_2O_2. Green triangles indicate ratio values on adding 50 µM H_2O_2 after 0 min, followed by DTT addition after 1 min. For each case, flow cytometry readings were taken at indicated time points post-treatment (soon after 0 min or 1 min).

The treatments with H_2O_2 (10 mM) and DTT (10 mM) indicated that the dynamic range of Grx1-roGFP2 in HEK293T cells was ~4. The dynamic range indicates that the fluorescence ratio (408/488 ratio) of fully oxidized cells is four-times that of fully reduced cells. The sensor also showed a consistent increase in fluorescence ratio with increasing H_2O_2 concentrations in A549 cells. Interestingly, the 408/488 ratios of control or untreated and DTT-treated cells were very close, suggesting that Grx1-roGFP2 was nearly completely reduced under steady-state conditions in the cytoplasm. Notably, the sensor was capable of showing real-time responses to oxidant and reductant treatments swiftly, within one to two minutes.

3.3 Generation of redox biosensor expressing stable cell lines

Transient transfections with the redox biosensor were short lived, and therefore, cell lines stably expressing the biosensor were generated for further experiments. Lentivirus based gene delivery method was utilized. For this, pLVX-Grx1-roGFP2 plasmid (containing a lentiviral backbone), VSVg helper plasmid and Gag-pol packaging plasmid were co-transfected in HEK293T cells. These expressed in the cells to form Grx1-roGFP2 expressing lentiviruses, which were collected and filtered out from the supernatant. pLX-GFP plasmid was used along with the helper plasmids (VSVg and Gag-pol) to make GFP expressing lentiviruses.

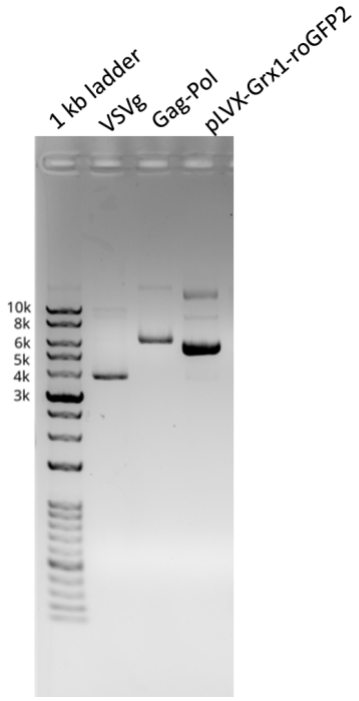

Sample	Concentration (ng/ul)
VSV-G	132.2
Gag-pol (Lenti)	189
pLVX-puro-Grx1-roGFP	522.5

Figure 9. Agarose gel electrophoresis of VSVg, Gag-pol and Grx1-roGFP2 plasmids. Lane 1 is showing ladder, lane 2 contains VSVg, lane 3 contains Gag-pol and lane 4 has Grx1-roGFP2. The plasmid concentrations are mentioned in the table.

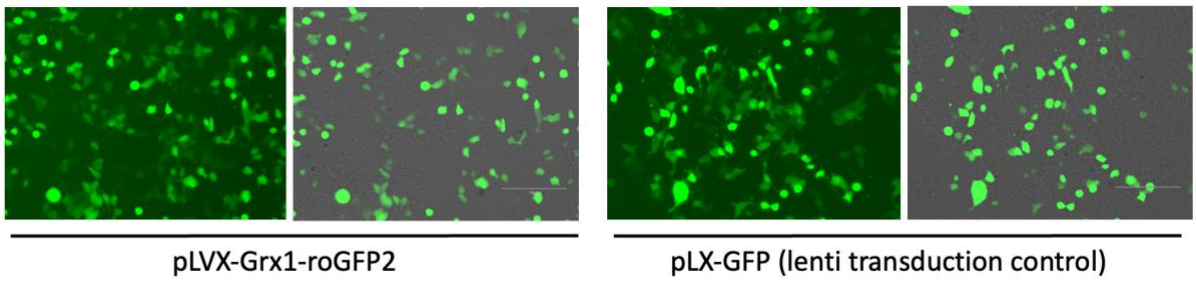

Figure 10. Lentivirus preparation. Images were taken day post co-transfection of target gene expressing pLVX-Grx1-roGFP2 plasmid, VSVg and Gag-pol, to form lentivirus. pLX-GFP was also co-transfected with VSVg and Gag-pol to form lentivirus. GFP expression was observed in both from the transfected target plasmids.

Prepared lentiviruses were used to transduce the target cell lines, which included the human lung epithelial (A549), human embryonic kidney (HEK293T) and Madin-Darby Canine Kidney (MDCK) cells. Lentiviruses can transduce dividing and non-dividing cells, and the target DNA integrates into the genome of the host cells. Therefore, post-transduction, the cells showing GFP expression indicated that the target gene (GFP or Grx1-roGFP2) became incorporated into the cell's genome.

pLX-GFP based lentivirus was used as a transduction control, to check for errors in the method in case of failure in transduction. Later, puromycin drug was added in the media of cells to select the Grx1-roGFP2 positive cells, since the lentiviral genome had puromycin resistance gene as a selectable marker. After every 48 hours, fresh media with puromycin was added and selection was continued until all un-transduced cells died. The Grx1-roGFP2 positive cells survived and were expanded to create stable cell lines.

A)

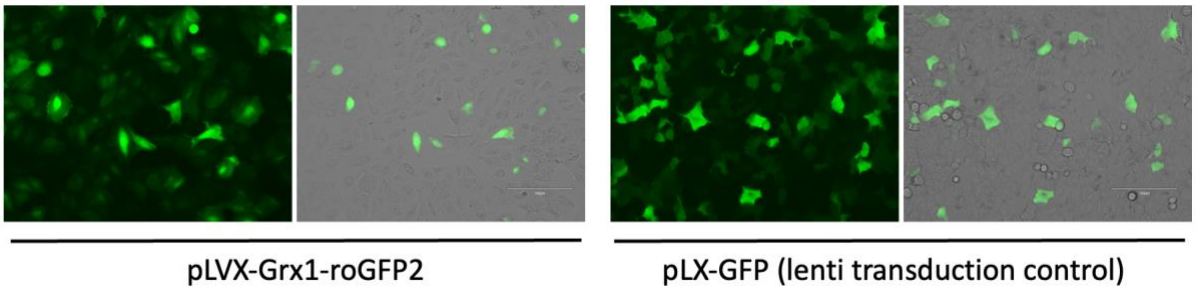

B)

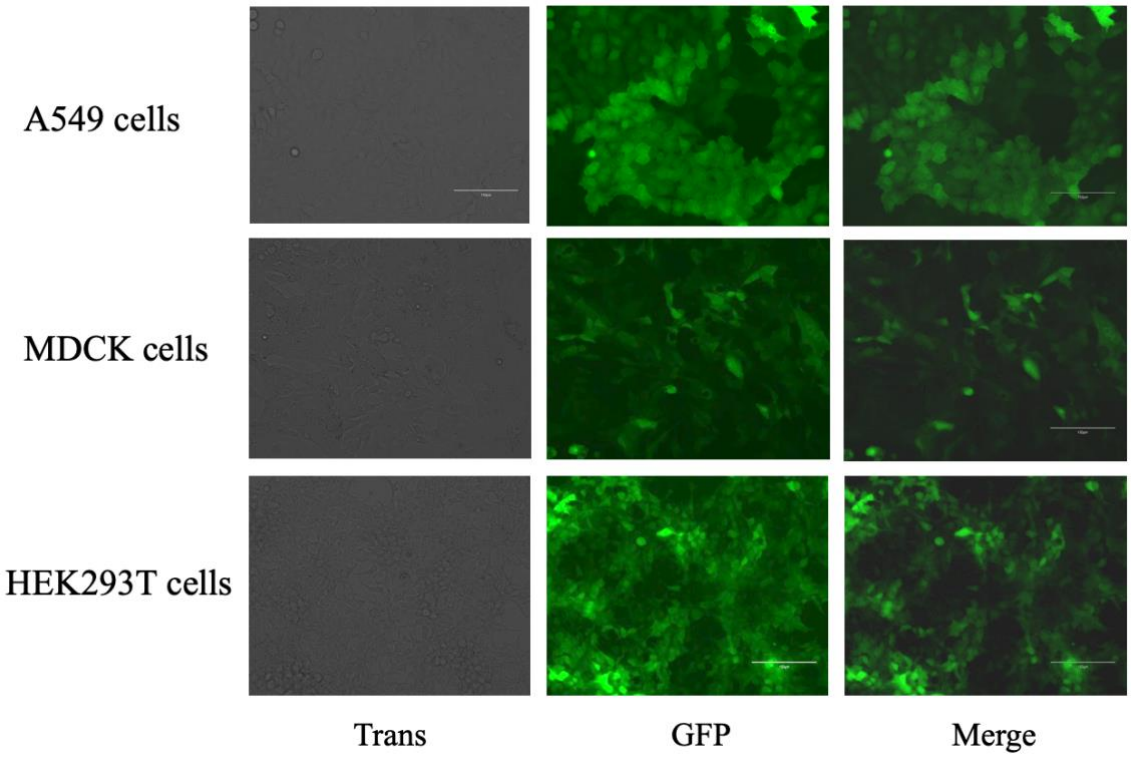

Figure 11. Grx1-roGFP2 expressing stable cell lines. (A) A549 cells one day post transduction, prior to selection. (B) A549, MDCK and HEK293T cells showing Grx1-roGFP2 expression after transduction and selection. Left panel is showing image in bright field, middle panel shows GFP positive cells, and the right panel is showing merged image.

3.4 Monitoring redox responsiveness of stable cells to oxidative stress

After generating the redox biosensor expressing stable cell lines, we investigated the real time changes in subcellular redox potential (E_{GSH}) of Grx1-roGFP2 expressing A549, MDCK and HEK293T cells upon H_2O_2 exposure. To do this, stable A549, MDCK and HEK293T cells were treated with varying concentrations of H_2O_2 for 3 min, and the ratiometric sensor response was recorded. H_2O_2 mounts an oxidative stress within the cells, and the sensitivity of the cytosolic sensor towards different concentrations of the oxidizing agent can be assessed for each stable cell line.

A treatment of 10 mM of H_2O_2 is tolerable and sufficient to attain complete oxidation of cells, and higher concentrations are toxic. Also, 20 mM DTT leads to complete reduction of the redox status of the cell population. The cytosol usually maintains quite a reducing environment (GSH: GSSG ratio of ~ 3300:1). Therefore, the 408/488 ratio of DTT treated fully reduced cells shows a slight decrease on comparing against the ratio of control untreated cells.

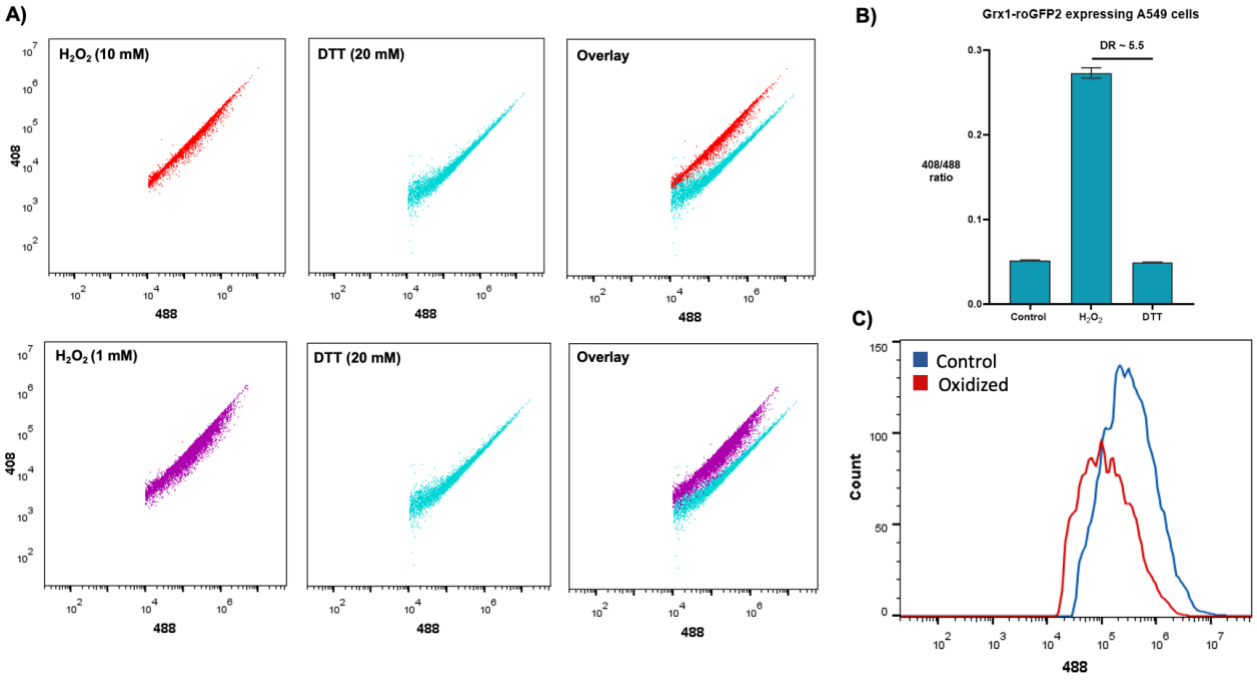

Figure 12. Response to oxidative and reductive stress. (A) Dot plots depict the ratiometric shift in biosensor response after complete oxidation, upon treatment with 10 mM H_2O_2, and with complete reduction, upon treatment with 20 mM DTT. The oxidized population shifted upward (increased fluorescence at 408 nm) and leftward (decreased

fluorescence at 488 nm), whereas the opposite was seen for reduced population, as expected. (B) The dynamic range (DR) of the sensor in A549 cells after complete oxidation and reduction by H_2O_2 and DTT, respectively. (C) Oxidative stress decreased the fluorescence at 488 nm with constant emission of 525 nm, compared to control untreated cells. A549 cells expressing the redox biosensor were treated with varying DTT or H_2O_2 for 3 min before the sensor responses were recorded in each case.

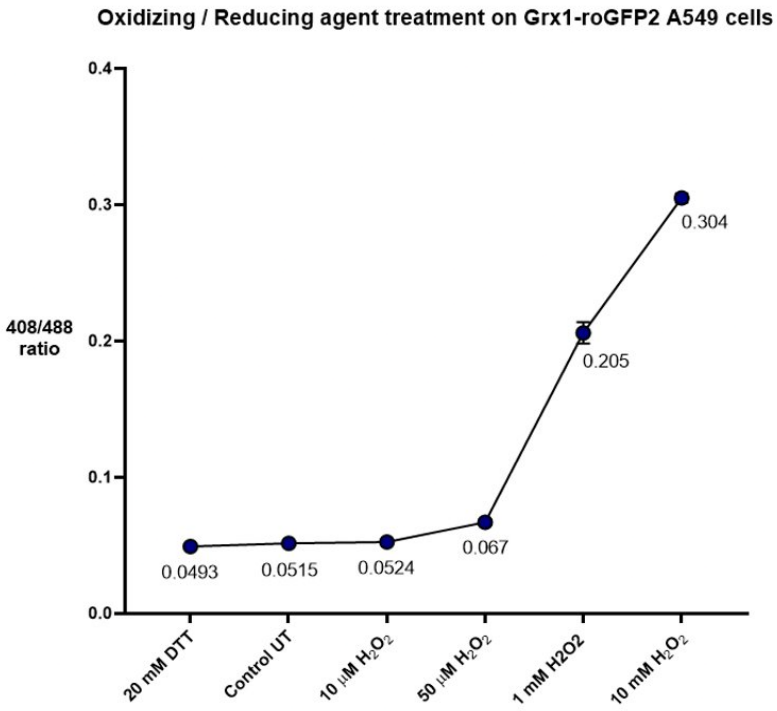

Figure 13. Redox responsiveness of A549 stable cells. Graph depicts redox responses Grx1-roGFP2 expressing A549 cells toward DTT and increasing concentrations of H_2O_2.

A549 cells showed a fluorescence ratio (408/488 ratio) of ~0.05 in their basal state, in the absence of a treatment. Grx1-roGFP2 oxidation-reduction kinetics upon treatment with a low concentration of H_2O_2 (50 µM) showed low change in the fluorescence ratio in case A549 cells. A treatment with ~1 mM of H_2O_2 for 3 min lead to nearly 70% oxidation of Grx1-roGFP2 in A549 cell cytoplasm. Upon complete oxidation (408/488 ratio ~ 0.3), the fluorescence ratio showed a 6-fold increase compared to the basal level ratio, indicating a strong sensor response. Oxidation with 1 mM H_2O_2 corresponded to an E_{GSH} (glutathione redox potential) of -265 mV in A549 cells, whereas 50 µM H_2O_2 treatment corresponded to E_{GSH} = -315 mV.

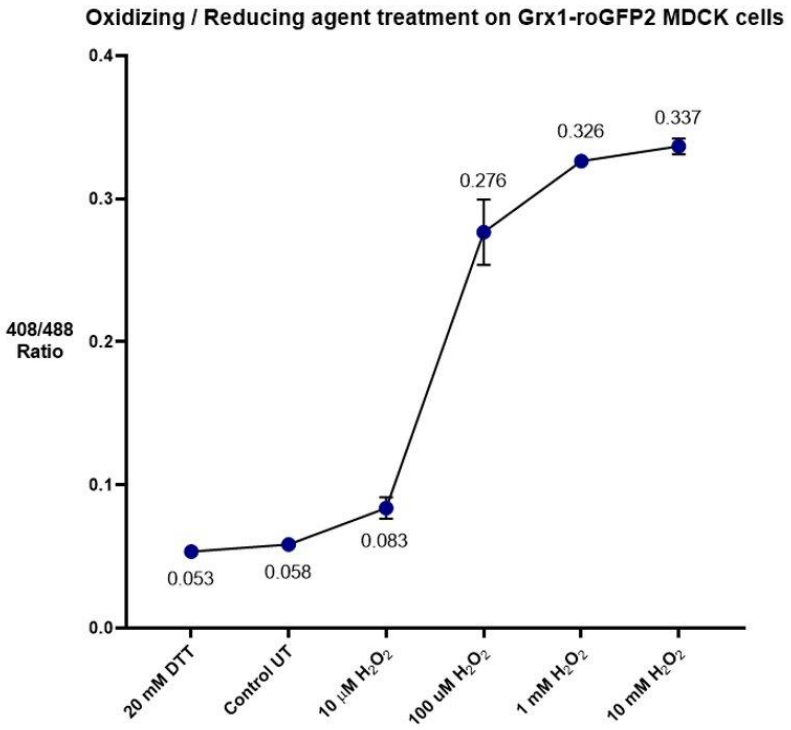

Figure 14. Redox responsiveness of MDCK stable cells. Graph depicts redox responses Grx1-roGFP2 expressing MDCK cells toward DTT and increasing concentrations of H_2O_2.

The basal state fluorescence ratio (408/488 ratio = ~0.05) of MDCK (Madin-Darby canine kidney) cells was similar to A549 cells. However, differences between MDCK and A549 cells is also apparent. Low millimolar concentration of H_2O_2 also lead to a decent increase in the degree of Grx1-roGFP2 oxidation and ~100 μM of H_2O_2 caused about 80% oxidation of Grx1-roGFP2 in MDCK cells. Comparable response was seen only upon a ~10-fold higher concentration of H_2O_2 (1 mM) in A549 cells. Treatment with 100 μM H_2O_2 lead to a significantly oxidized E_{GSH} of -250 mV, close to the fully oxidized E_{GSH} = -240 mV.

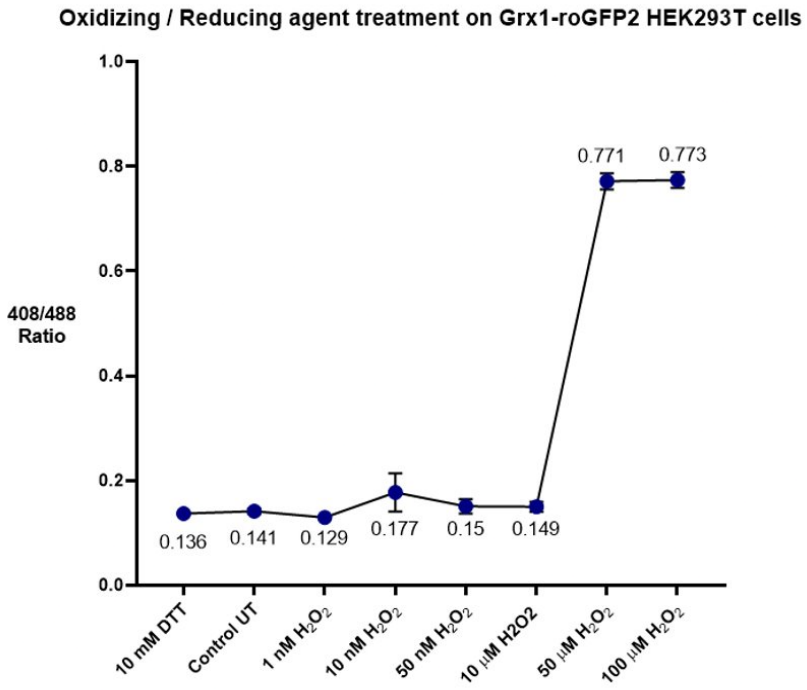

Figure 15. Redox responsiveness of HEK293T stable cells. Graph depicts the redox responses Grx1-roGFP2 expressing HEK293T cells towards DTT and increasing concentrations of H_2O_2.

The cytosol of HEK293T cells showed only a fractional change in the degree of Grx1-roGFP2 oxidation in response to nanomolar and low millimolar (10 µM) H_2O_2 concentrations, with approximate E_{GSH} = -314 mV. Lower sensitivity of the sensor at low nanomolar H_2O_2 concentrations is suggestive of an efficient anti-oxidative cellular response. However, it was interesting to observe that a treatment with ~50 µM of H_2O_2 for 3 minutes was enough to cause nearly complete oxidation (408/488 ratio = ~0.77) of Grx1-roGFP2 in HEK293T cells. This demonstrates that the cell line has a higher capability to metabolize H_2O_2, achieved by efficiently converting it into GSSG, a reaction that is likely facilitated by the presence of endogenous glutathione peroxidases.

3.5 Dynamic redox changes post Influenza A virus infection in stable cell lines

Next, we aimed to examine how Influenza virus infection affects the redox modulation of specific cell types. Influenza research often employs Madin-Darby

Canine Kidney (MDCK) cells due to their susceptibility to infection by various influenza virus strains. Meanwhile, A549 is a human lung adenocarcinoma cell line that has been extensively used in influenza A virus *in vitro* studies, although some influenza A strains have been found to be less effective in infecting these cells.

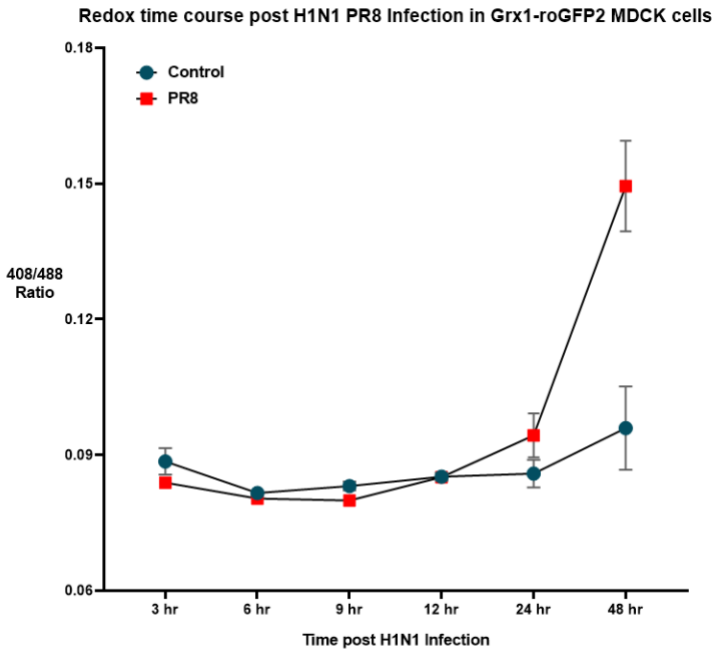

A)

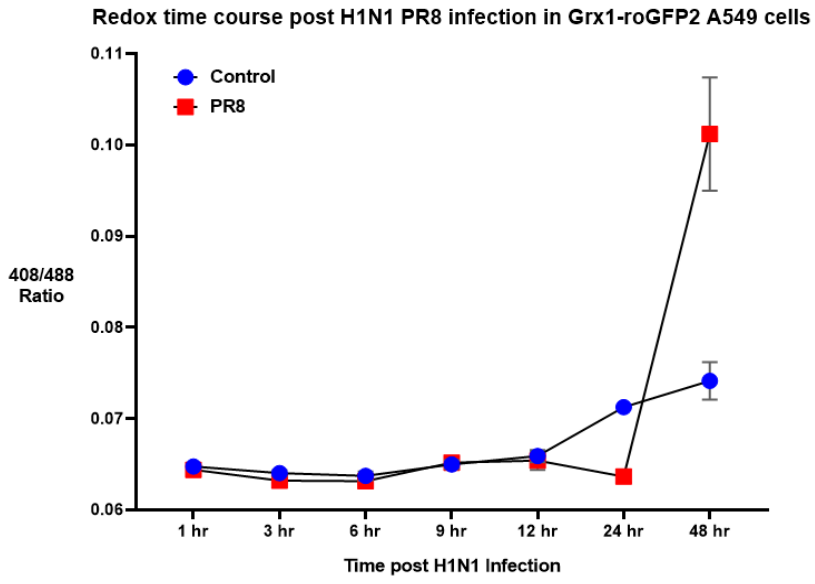

B)

Figure 16. Temporal redox response of IAV (PR8) infected Grx1-roGFP2 expressing cells. Graphs show 408/488 ratio after H1N1 PR8 infection in MDCK cells (A) and A549 cells (B) at the indicated time points.

Given that the redox conditions in A549 cells differed slightly from that in MDCK cells, we studied redox response of MDCK and A549 cells infected by H1N1 PR8 virus. Post influenza virus infection at 5 MOI, the fluorescence ratio (408/488) was measured at 3, 6, 9, 12, 24, and 48 hours post infection (h.p.i.).

PR8 infection at the same multiplicity of infection could induce higher oxidative stress (408/488 ratio ~0.15) in MDCK cells, as opposed to A549 cells (408/488 ratio ~0.10) at 48 hours post infection. PR8 infection induced a substantial oxidative shift in E_{GSH} of MDCK cytosol at 48 hours (+18 mV), compared with 12 hours post infection. The redox potential E_{GSH} at 48 h.p.i. was -274 mV, whereas at it equalled -292 mV at 12 h.p.i.. In A549 cells, the E_{GSH} was -290 mV at 48 h.p.i., corresponding to a (+11 mV) oxidative shift compared to the control redox potential. There was a reductive shift (-6.5 mV) in the E_{GSH} in PR8 infected A549 cells compared to uninfected cells, at 24 hours post infection.

3.6 Influenza virus strain-specific redox modulation in A549 cells

Redox biosensor expressing A549 cells were then infected with different strains of Influenza A virus, to investigate strain-specific temporal redox modulations in infected cells. Grx1-roGFP2 expressing A549 cells were infected with H1N1 (PR8) (A/Puerto Rico/8/1934), the seasonal influenza A virus H3N2 (A/Wisconsin/15/2009), and the human isolate of avian influenza H5N1 (A/Vietnam/1203/2004), which lacks the polybasic cleavage site (termed HALo) at 5 MOI.

At differing time points post infection, mean 408/488 ratios were recorded by flow cytometry to estimate the degree of Grx1-roGFP2 sensor oxidation. Thus, we could infer the redox status and extent of ROS accumulation in virus infected cells upon comparing against the uninfected control cells at each time point. The virus entry takes place in around 1 hour, then virus replication takes place, and virus particles can exit the cell after around 12 hours, to lead to multi-cycle infections at further time points. Uninfected Grx1-roGFP2 A549 cells displayed a significantly reduced cytoplasm (408/488 ratio, ~0.055 to 0.065). Post influenza virus infection, the fluorescence ratio was measured at 3, 6, 9, 12, 24, and 48 hours post infection (h.p.i.).

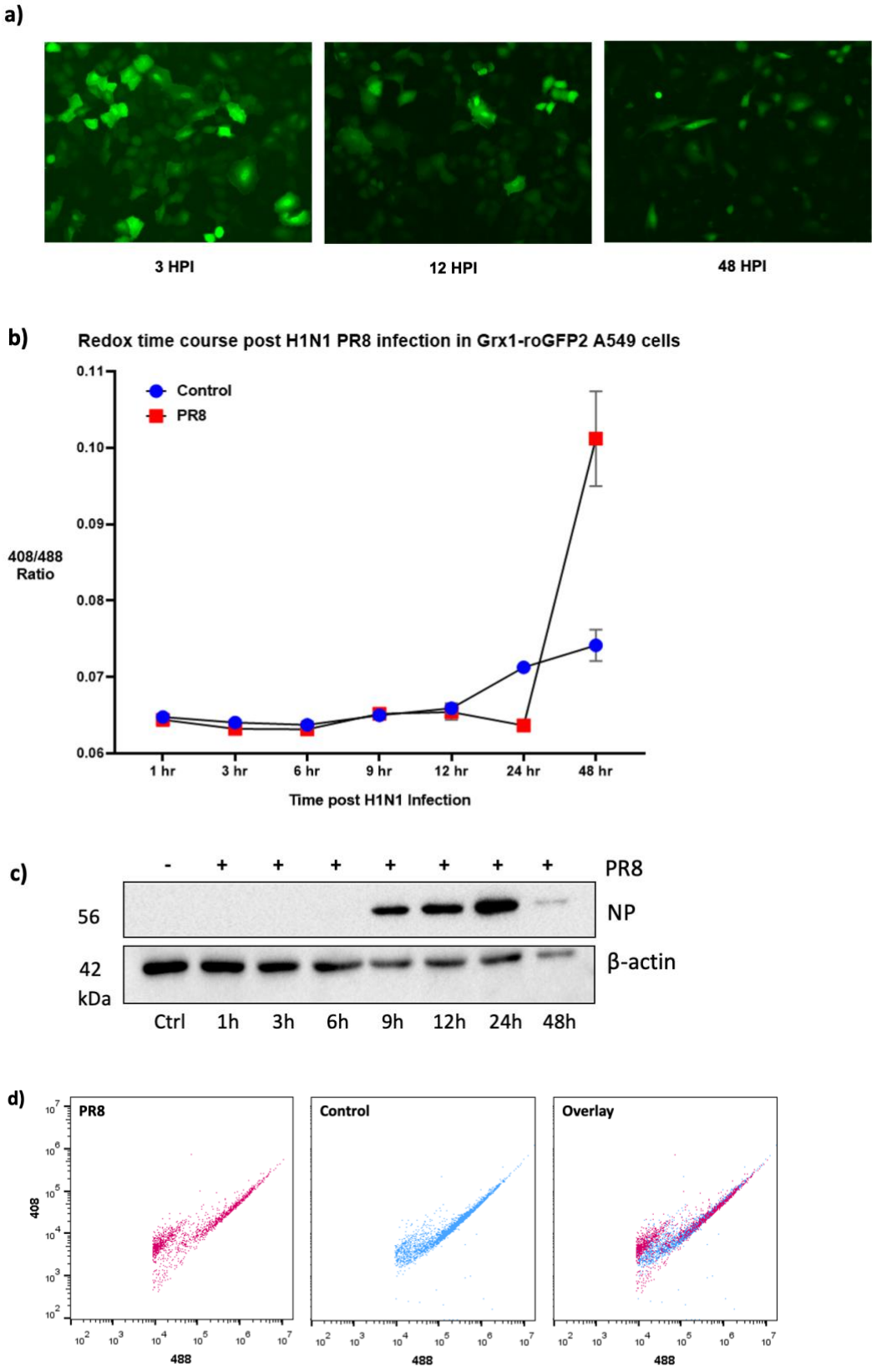

Figure 17. Temporal redox response of H1N1 (PR8) infected Grx1-roGFP2 expressing A549 cells. (a) Microscopy images of virus infected cells at 3 hours, 12 hours and 48 hours post infection. (b) Graph depicts the fluorescence ratio of control and infected cells at the

indicated time points post-infection. (c) Virus levels assessed by intracellular nucleoproteins (NP) expression over the course of infection. (d) Dot plots depict the ratiometric shift in biosensor response for H1N1 infected cells at 48 h.p.i. as compared to control population.

Upon infection with H1N1 (PR8) in A549, as mentioned earlier, infection did not induce significant redox changes at early time points, as detected by the biosensor. At 24 h.p.i., however, the infected cells show a reduced status, and the fluorescence ratio remarkably increased at 48 h.p.i. (408/488 ratio, ~0.1) compared with that in the control cells, showing a highly oxidized status.

The seasonal Influenza H3N2 virus did not cause significant changes in the redox status of A549 cells at any time point during its replication cycle.

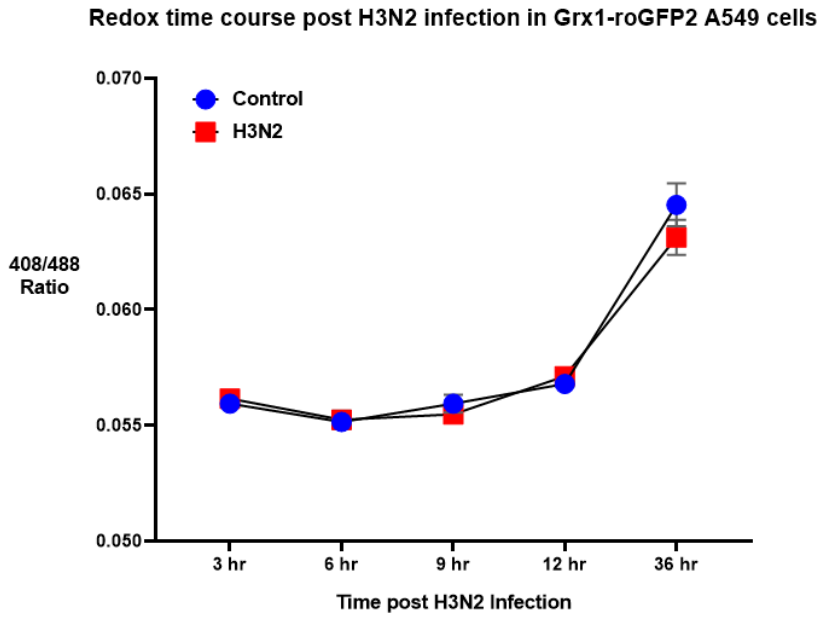

Figure 18. Temporal redox response of H3N2 infected Grx1-roGFP2 expressing A549 cells. Graph depicts the fluorescence ratio of control and infected cells at the indicated time points post-infection.

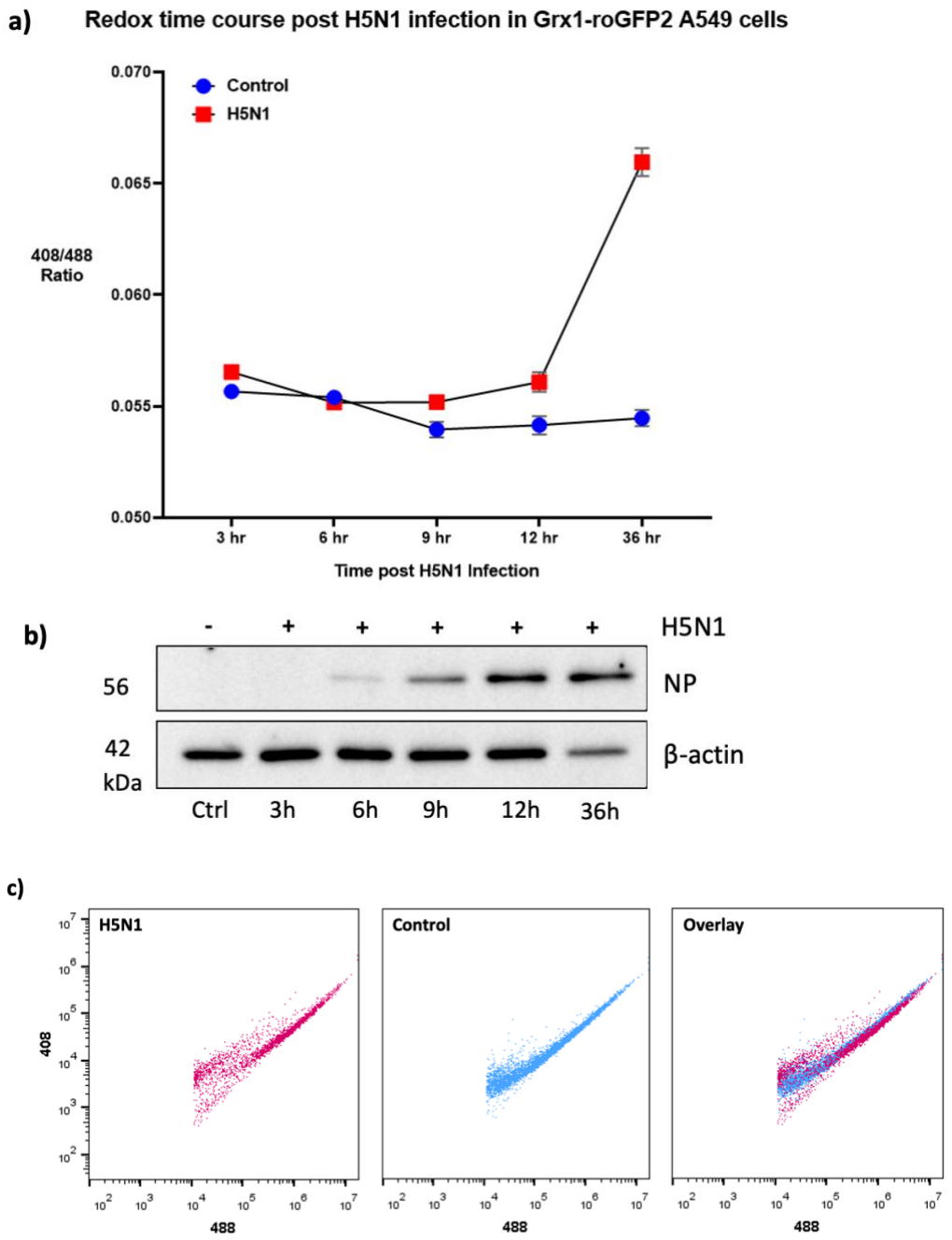

Figure 19. Temporal redox response of H5N1 infected Grx1-roGFP2 expressing A549 cells. (a) Graph depicts the fluorescence ratio of control and infected cells at the indicated time points post-infection. (b) Virus levels assessed by intracellular nucleoproteins (NP) expression over the course of infection. (c) Dot plots depict the ratiometric shift in biosensor response for H1N1 infected cells at 48 h.p.i. as compared to control population.

H5N1 infected cells interestingly showed a slightly oxidized status at 3 h.p.i. followed by reduction at 6 h.p.i. Subsequently, H5N1 infected cells demonstrated increased biosensor oxidation ratio over time. H5N1 induced an oxidative stress starting from 9

h.p.i, which progressively increased across later time points. The redox potential, E_{GSH} was -305.8 mV at 36 hours post infection. This suggests that both H1N1 and H5N1 viruses could increase intracellular ROS. Important to note that H5N1 infection caused biosensor oxidation at early time points as well (3, 9 and 12 h.p.i.), whereas H1N1 showed significant redox modulation only at later time points (24 and 48 h.p.i.), possibly during multicycle infections. Moreover, H5N1 had a faster replication kinetics and showed NP expression even at 6 h.p.i., as opposed to 9 h.p.i. for the H1N1 virus. However, the results suggested that H1N1 influenza virus induced intense ROS production and was overall a stronger inducer of oxidative stress than H5N1 virus.

3.7 Screening viral proteins for redox perturbation

Next, we attempted to screen the Influenza viral proteins for their involvement in modulating cellular redox. To begin with, eight viral proteins (i.e. HA, NA, NP, M, PA, PB1, PB2 and NS, which represent all of the viral proteins) of the Influenza A virus H1N1 subtype PR8 (A/Puerto Rico/8/1934) were individually expressed in Grx1-roGFP2 expressing HEK293T cells, with the help of plasmid transfection. This strategy will help identify viral redox-modulating components, for which the mechanism can further be investigated.

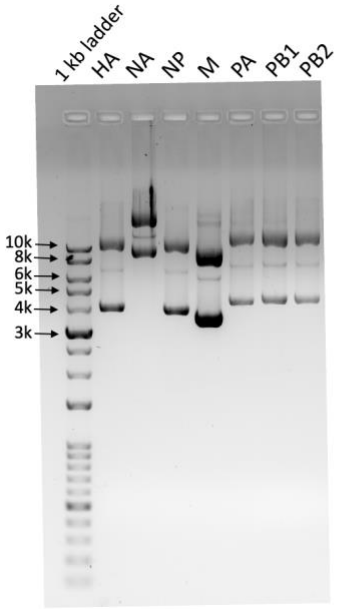

Sample	Concentration (ng/ul)
pDZ-PR8-HA	193.4
pDZ-PR8-NA	227.8
pDZ-PR8-NP	407.5
pDZ-PR8-M	489.9
pDZ-PR8-PA	251
pDZ-PR8-PB1	243.4
pDZ-PR8-PB2	276

Figure 20. Gel electrophoresis image for PR8 virus plasmids. The viral genes were in a bidirectionally expressing backbone, pDZ. The concentration of viral plasmids was recorded.

The redox status was detected at 36 hours post-transfection by flow cytometry, by assessing the degree of Grx1-roGFP2 sensor, for each viral protein. An empty vector, pDZ, which was the same as the backbone in viral plasmids, was used as a transfection control to observe redox-related effects due to the process of transfection. Compared to this control, an increase in the fluorescence ratio (408/488) represented oxidation, and decrease in the ratio represented a reduction in the microenvironment of cells, due to overexpression of the specific viral protein.

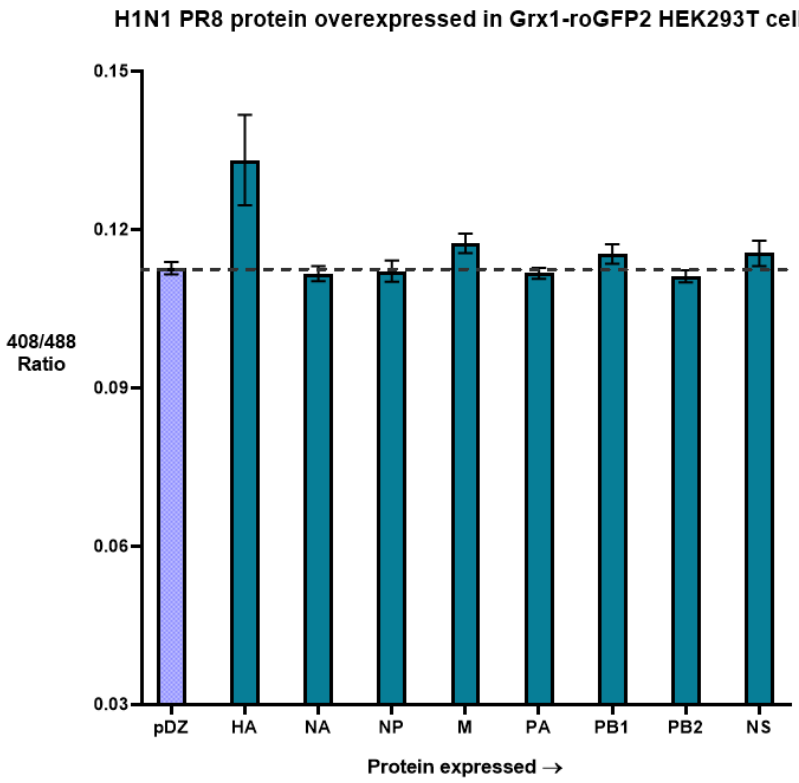

Figure 21. H1N1 PR8 proteins overexpressed in HEK293T stable cells. PR8 plasmids were transfected in Grx1-roGFP2 expressing HEK293T cells and fluorescence ratio was recorded at 36 hous post-transfection. The dashed line indicated fluorescence ratio of empty vector control.

The HA (hemagglutinin) viral protein showed a perturbation in cellular redox status and caused oxidation. Further, we went on to test the redox response of these viral protein expressing cells to an oxidative stress - whether they resisted or supported oxidation. This was estimated by treating harvested cells at 36 hours post transfection with 10 µM H_2O_2 for 3 min.

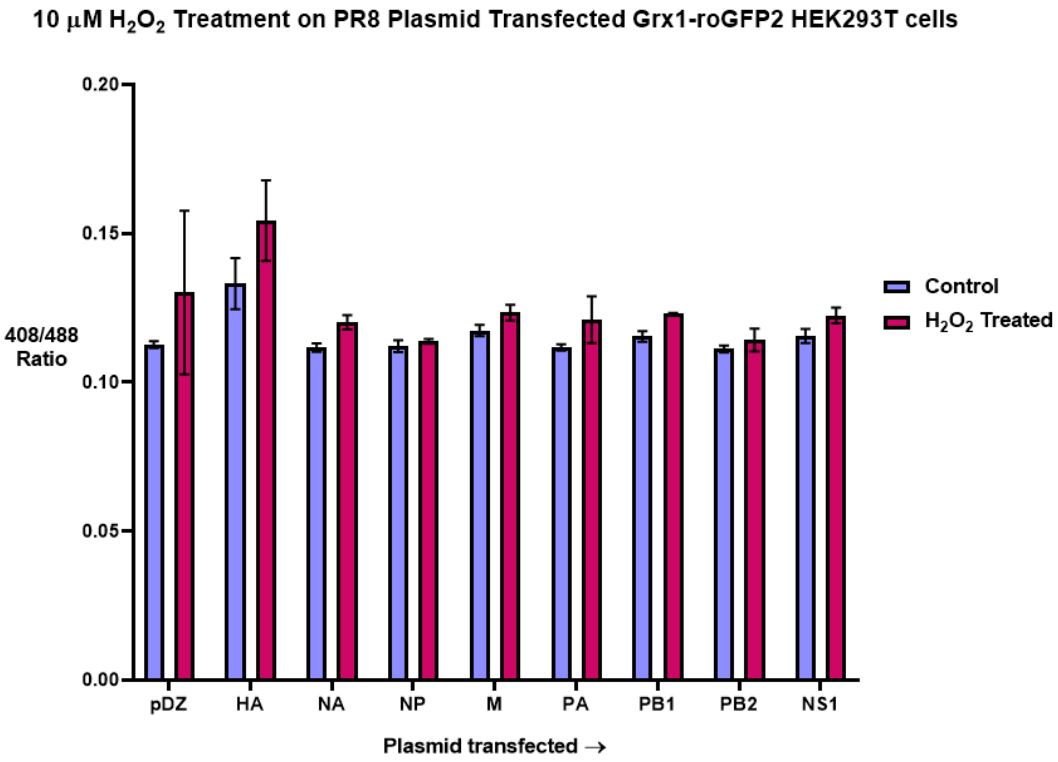

Figure 22. H1N1 PR8 proteins overexpressed in HEK293T stable cells followed by H_2O_2 treatment. PR8 plasmids were transfected in Grx1-roGFP2 expressing HEK293T cells and at 36 hous post-transfection, cells were treated with 10 μM H_2O_2 for 3 minutes and the fluorescence ratio was recorded.

Although the experiment requires repetition due to high standard deviation in controls, it is notable that HA expressing cells were highly oxidized (408/488 ratio ~0.15), compared to the other viral proteins expressing cells (408/488 ~0.12), given the same exogenous H_2O_2 treatment. This suggests that hemagglutinin (HA) protein could promote an oxidative stress, which is associated with H1N1 Influenza virus infection.

To validate the finding for H1N1 influenza virus, we overexpressed the viral proteins (i.e. HA, NA, NP, M, PA, PB1, PB2 and NS) of another Influenza A virus H1N1 subtype Cal/09 (A/California/04/2009), individually in Grx1-roGFP2 expressing HEK293T cells.

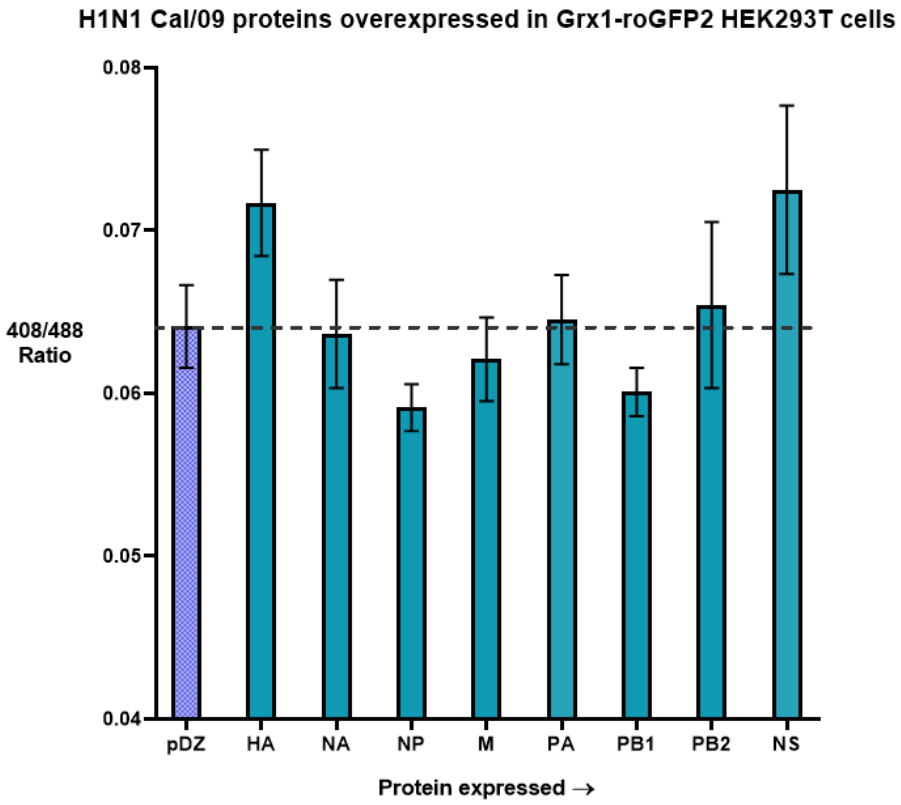

Figure 23. H1N1 Cal/09 proteins overexpressed in HEK293T stable cells. Cal/09 plasmids were transfected in Grx1-roGFP2 expressing HEK293T cells and fluorescence ratio was recorded at 36 hous post-transfection. The dashed line indicated fluorescence ratio of empty vector control.

Interestingly, in the screen, the HA (hemagglutinin) viral protein demonstrated oxidation in redox sensor expressing cells. NS (non-structural) protein overexpression showed relative oxidation in the HEK293T cells as well. We explored a redox response of these viral protein expressing cells to a reductive stress this time. This was estimated by treating cells at 36 hours post transfection with the reducing agent DTT (10 mM) for 3 min.

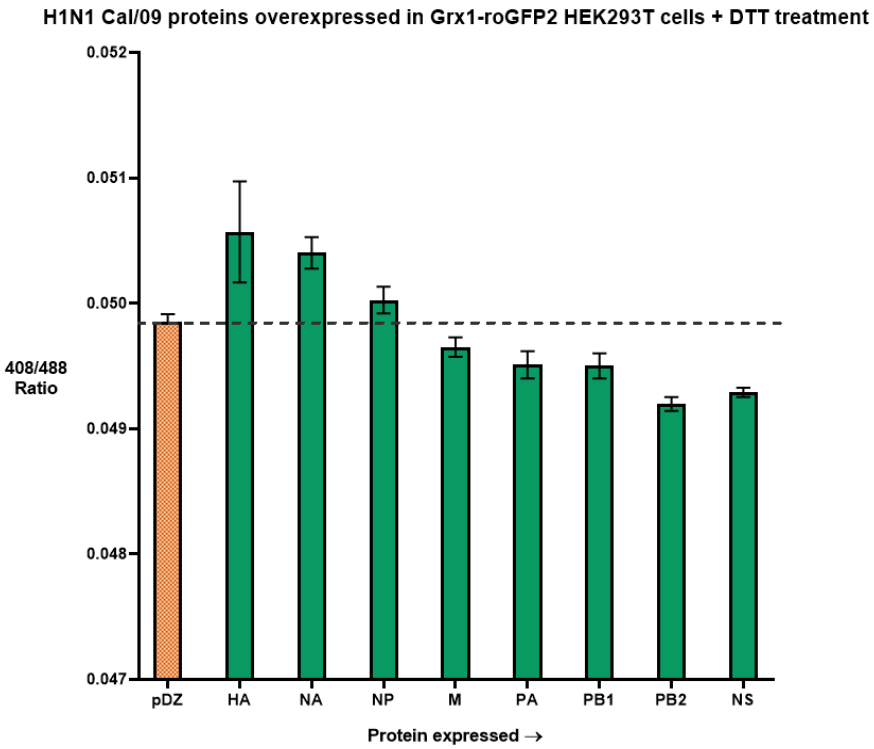

Figure 24. H1N1 Cal/09 proteins overexpressed in HEK293T stable cells followed by DTT treatment. Cal/09 plasmids were transfected in Grx1-roGFP2 expressing HEK293T cells and at 36 hous post-transfection, cells were treated with 10 mM DTT for 3 minutes and then fluorescence ratio was recorded. The dashed line indicated fluorescence ratio of empty vector control.

The control cells, as well as many viral protein overexpressing cells, demonstrated a reduced redox status. However, we observed that HA protein expressing cells showed an oxidized redox status, compared to the control cells. This suggests that HA could resist reductive stress as well, to promote oxidation. However, these experiments need to be repeated to arrive at a conclusive trend.

3.8 Engineering red fluorescent Influenza virus

Next, we were motivated to look into the relative contributions of infected versus uninfected bystander cells on the redox modulations observed, and to differentiate the redox status of the two populations. To achieve this, we began engineering a recombinant - red fluorescent - Influenza virus. The red virus could then be utilized to trace IAV infections, upon infecting the green fluorescent, Grx1-roGFP2 biosensor

expressing stable A549 cells. With the help of flow cytometry, we can assess the redox biosensor response precisely in virus infected - red fluorescent population of cells, versus the remaining uninfected - green fluorescent cells.

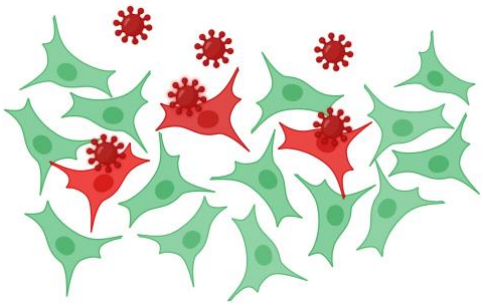

Figure 25. Infected versus bystander cells. The schematic shows the basic strategy to differentiate virus infected and bystander cells, where red fluorescent Influenza virus will be used to infect the Grx1-roGFP2 expressing stable cells. Virus infected cells can be distinguished with flow cytometry.

3.8.1. Cloning for inserting RFP in Influenza viral gene

To begin engineering a red fluorescent Influenza virus, the strategy was to clone the red fluorescent protein (RFP) gene within the NS (non-structural) gene segment of Influenza virus, as mentioned earlier in the methods section. PCR reaction for NS1, RFP and NEP genes was set up with the help of the respective forward and reverse primers, and templates mentioned in Table 1. Gradient PCR was performed to determine optimum annealing temperature. We used the high fidelity Phusion DNA polymerase.

A)

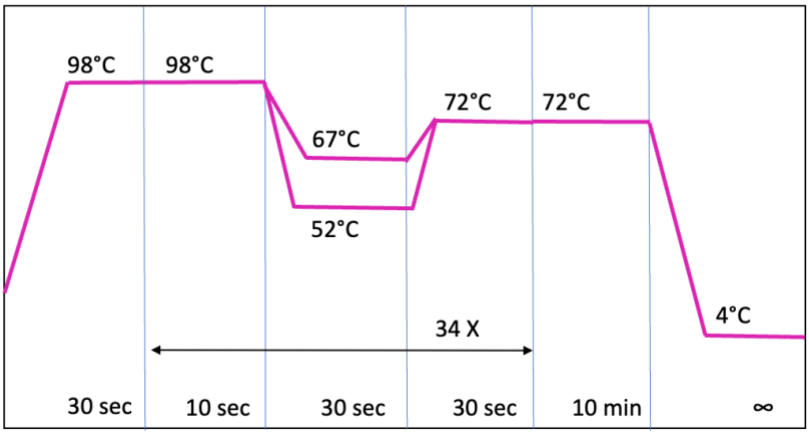

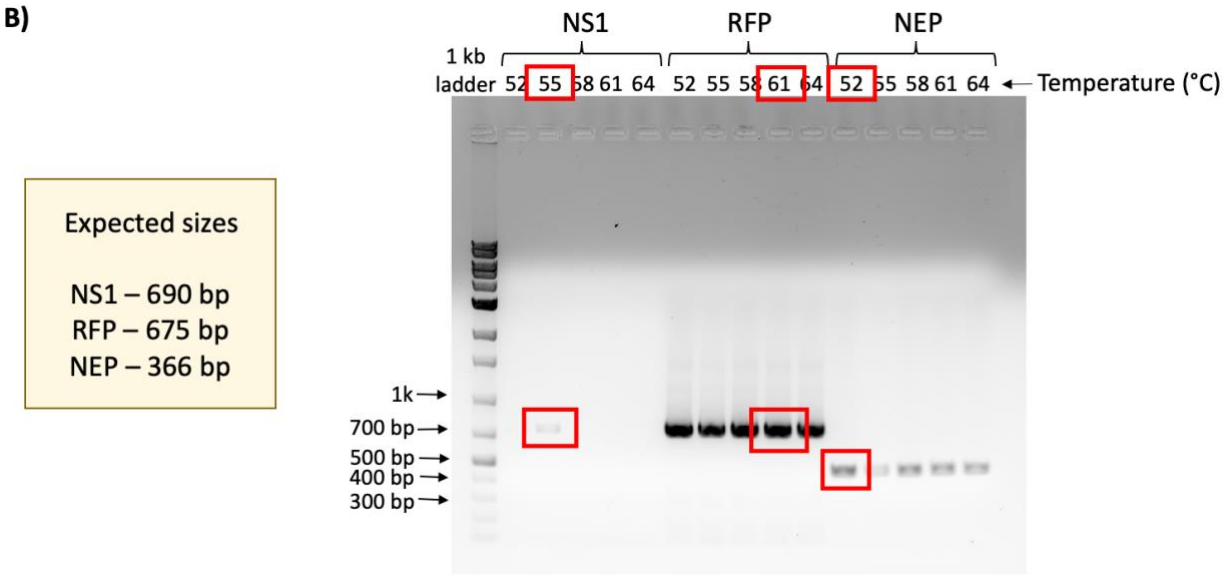

Figure 26. Gradient PCR for NS1, RFP and NEP. (A) Thermal cycling temperature profile for PCR. (B) Temperature gradient PCR products for NS1, RFP and NEP genes. Different annealing temperatures (52-64 °C) were tested and chosen temperatures based on products are boxed in red colour.

After selecting annealing temperatures - 55°C for NS1, 61°C for RFP and 52°C for NEP - the genes were PCR amplified. PCR amplification was followed by gel purification. Since the primers were designed to cause incorporation of overlapping sequences in PCR products, we next performed overlap extension PCR for NS1 and RFP together, and RFP and NEP together (Bryksin and Matsumura, 2010).

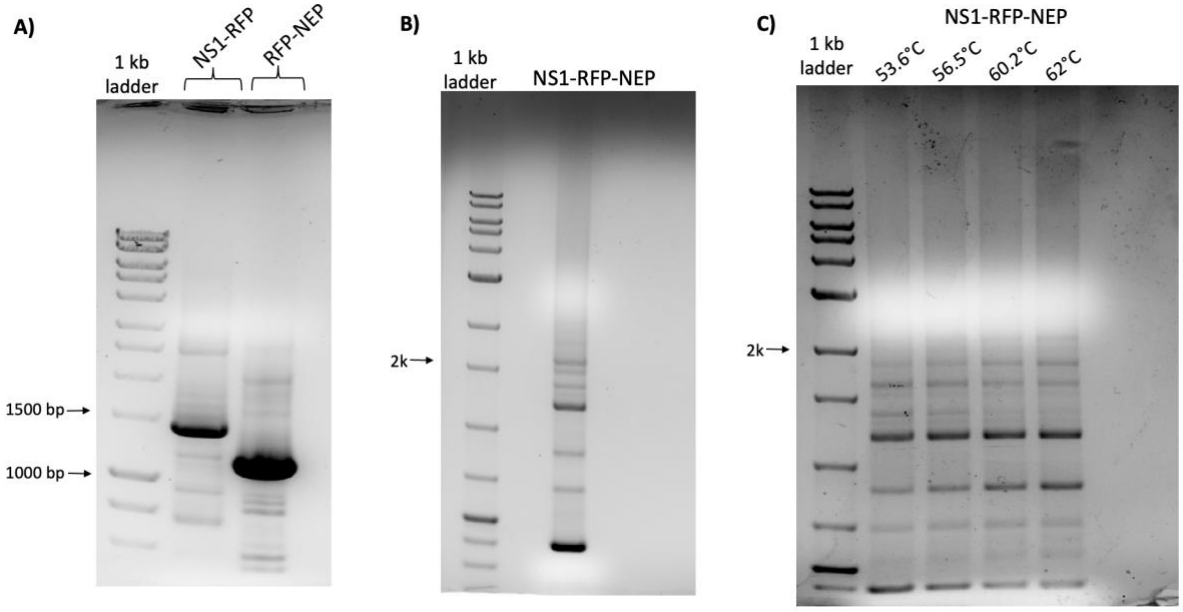

Figure 27. Overlap extension PCR to construct NS1-RFP-NEP cassette. (A) shows the overlap extension products of NS1 + RFP PCR, and RFP + NEP PCR. The products were at expected sizes of 1.4 kb and 1.1 kb. (B) shows the overlap extension product of NS1-RFP + RFP-NEP PCR. The expected product NS1-RFP-NEP was 1.8 kb in size. Very faint band was observed at desired size. (C) shows temperature gradient PCR, at mentioned annealing temperatures, for NS1-RFP + RFP-NEP PCR to form NS1-RFP-NEP product.

NS1-RFP and RFP-NEP products were PCR amplified and utilized for an overlap extension PCR to form NS1-RFP-NEP cassette. However, only faint bands were observed at the desired product size of 1.8 kb. The product was not obtained on performing PCR with different annealing temperatures either. Hence, further troubleshooting is required.

Going further, once NS1-RFP-NEP cassette is formed, it will be digested with SapI restriction digestion enzyme, along with the pDZ backbone, and ligated in the vector backbone. The rest of the Influenza virus genes (HA, NA, NP, M, PA, PB1, PB2) expressed in pDZ plasmid will then be co-transfected with RFP-NS to rescue RFP recombinant IAV using reverse genetics system .

To rescue viable virus, it is necessary for cells to express both negative sense genome and positive sense transcripts of Influenza A virus (IAV). Thus, a bidirectional or ambisense plasmid system pDZ is utilized, to incorporate an RNA Polymerase I promoter and RNA Polymerase II promoter, flanking all influenza genes.

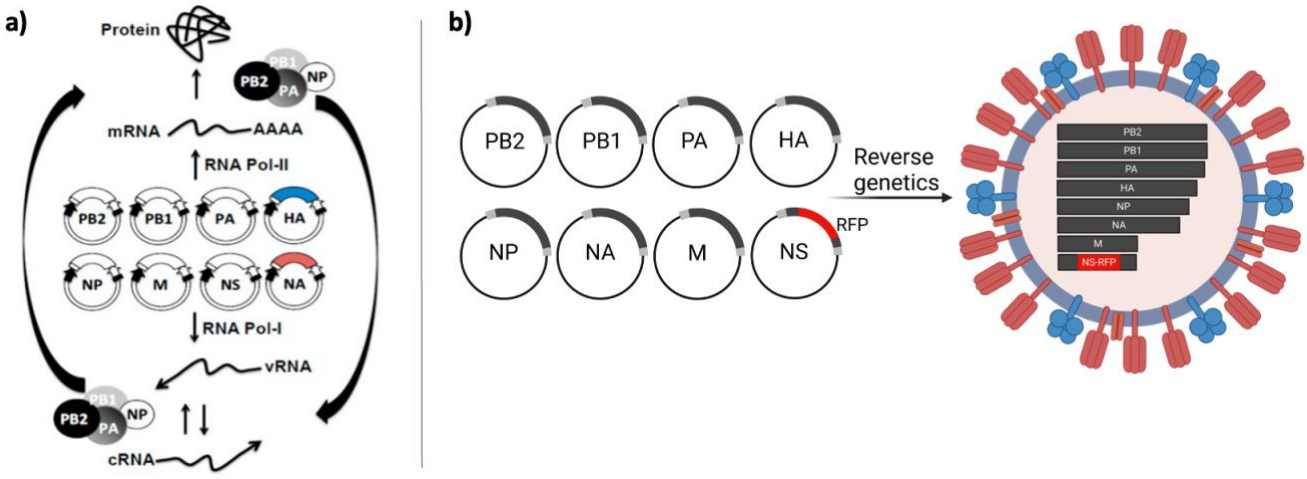

Figure 28. Reverse genetics strategy. (a) After co-transfection with IAV rescue plasmids, RNA Pol I produces the negative sense vRNAs (bottom) whereas RNA Pol II causes production of the eight viral mRNAs (top) which get translated into virus proteins (Adapted from *Int. J. Mol. Sci. 2017*). (b) RFP inserted NS used with other rescue plasmids to engineer red fluorescent Influenza A virus.

4. Discussion

The advancement of basic research in the field of IAV biology is hindered due to the unavailability of tools to accurately investigate the physiological changes in IAV-infected cells during various phases of infection. In our study, we employed a genetically encoded sensor, consisting of human glutaredoxin-1 connected to a redox-sensitive green fluorescent protein (Grx1-roGFP2), to precisely measure the glutathione redox potential (E_{GSH}) in the cytosol of Influenza A virus-infected cells over the course of infection.

By employing the Grx1-roGFP2 redox probe, we observed dynamic fluctuations in cytosolic glutathione redox potential. The biosensor oxidation triggered by H_2O_2 was found to be higher in HEK293T cells compared to A549 and MDCK cells, indicating different oxidative responses among various cell types. Remarkably, the redox biosensor exhibited rapid detection of changes in the fluorescence ratio of Grx1-roGFP2 due to oxidation and reduction, within a minute.

A significant amount of research has suggested that IAV infection results in the accumulation of oxidative stress, and antioxidant treatments have been proposed. Our results also showed oxidative stress in infected cells during later stages of infection. We compared the effects of influenza virus strains and found that the human isolate of avian H5N1 IAV induced oxidation earlier than H1N1 virus, beginning at 9 hours post-infection. However, H1N1 infection caused a higher increase in biosensor oxidation ratio after 24 hours, resulting in an E_{GSH} shift of approximately +16 mV greater than H5N1 infection in A549 cells.

Several IAV proteins have been shown to regulate redox-sensitive signaling pathways, leading to ROS generation and oxidative stress. However, their interactions with host cell factors are still not clear. In our investigation of IAV

proteins, we consistently observed an oxidized response to the redox sensor in cells overexpressing the H1N1 hemagglutinin (HA) protein. HA is a crucial immunogen for vaccine development, and it plays a vital role in virus entry and host tropism. Interestingly, HA is a homo-trimer that undergoes oxidative folding and disulphide bond formation. Further studies are needed to determine whether HA actually promotes the oxidation of cellular environment to aid its folding process.

Influenza A virus infection involves multiple stages that can alter the cellular redox status, causing oxidative stress and inflammation. However, we have limited knowledge regarding whether the redox modulation is a viral function to promote viral replication or a defensive response generated by cells after detecting infection. Understanding the mechanisms by which IAV regulates redox status can provide insights into the pathogenesis of IAV infection and help identify potential targets for antiviral therapies. Further research is necessary to elucidate the complex interplay between IAV and host cell redox signaling pathways and develop effective strategies for preventing and treating influenza virus infections.

5. Future Directions

Future work includes troubleshooting the cloning of red fluorescent protein (RFP) gene within IAV genome. Red fluorescent recombinant IAV will be instrumental in distinguishing the redox response of virus infected and bystander cells, which will provide important information to improve our understanding of the redox regulation within cells after a few cells get infected. Further, we intend to study the redox modulation within other cellular compartments like the mitochondria and endoplasmic reticulum, which house several important redox factors. Various IAV proteins localize in these organelles, for instance - HA folding occurs in the ER. Thus, gaining insights into the modulation of mitochondria and ER redox status by IAV proteins will be crucial to narrow down on the viral culprits responsible for organelle specific, and cellular redox modulation, for the virus' benefit. Ultimately, the redox biosensor can be equipped in animal models, to challenge the animals with IAV infection and study the redox perturbations *in vivo*.

References

1. Abo, A, Pick, E, Hall, A, Totty, N, Teahan, CG, and Segal, AW (1991). Activation of the NADPH oxidase involves the small GTP-binding protein p21rac1. Nature 353, 668–670.

2. Albrecht, SC, Sobotta, MC, Bausewein, D, Aller, I, Hell, R, Dick, TP, and Meyer, AJ (2014). Redesign of genetically encoded biosensors for monitoring mitochondrial redox status in a broad range of model eukaryotes. J Biomol Screen 19, 379–386.

3. Allen, JD, and Ross, TM (2018). H3N2 influenza viruses in humans: Viral mechanisms, evolution, and evaluation. Hum Vaccin Immunother 14, 1840–1847.

4. Amatore, D, Sgarbanti, R, Aquilano, K, Baldelli, S, Limongi, D, Civitelli, L, Nencioni, L, Garaci, E, Ciriolo, MR, and Palamara, AT (2015). Influenza virus replication in lung epithelial cells depends on redox-sensitive pathways activated by NOX4-derived ROS. Cell Microbiol 17, 131–145.

5. Baudin, F, Petit, I, Weissenhorn, W, and Ruigrok, RWH (2001). In Vitro Dissection of the Membrane and RNP Binding Activities of Influenza Virus M1 Protein. Virology 281, 102–108.

6. Bedard, K, and Krause, K-H (2007). The NOX Family of ROS-Generating NADPH Oxidases: Physiology and Pathophysiology. Physiological Reviews 87, 245–313.

7. Bogs, J, Veits, J, Gohrbandt, S, Hundt, J, Stech, O, Breithaupt, A, Teifke, JP, Mettenleiter, TC, and Stech, J (2010). Highly pathogenic H5N1 influenza viruses carry virulence determinants beyond the polybasic hemagglutinin cleavage site. PLoS One 5, e11826.

8. Boudreau, HE, Emerson, SU, Korzeniowska, A, Jendrysik, MA, and Leto, TL (2009). Hepatitis C Virus (HCV) Proteins Induce NADPH Oxidase 4 Expression in a Transforming Growth Factor β-Dependent Manner: a New Contributor to HCV-Induced Oxidative Stress. J Virol 83, 12934–12946.

9. Boulo, S, Akarsu, H, Ruigrok, RWH, and Baudin, F (2007). Nuclear traffic of influenza virus proteins and ribonucleoprotein complexes. Virus Res 124, 12–21.

10. Bouvier, NM, and Palese, P (2008). THE BIOLOGY OF INFLUENZA VIRUSES. Vaccine 26, D49–D53.

11. Bryksin, AV, and Matsumura, I (2010). Overlap extension PCR cloning: a simple and reliable way to create recombinant plasmids. BioTechniques 48, 463–465.

12. Cai, J, Chen, Y, Seth, S, Furukawa, S, Compans, RW, and Jones, DP (2003). Inhibition of influenza infection by glutathione. Free Radic Biol Med 34, 928–936.

13. Chamberlain, N et al. (2019). Lung epithelial protein disulfide isomerase A3 (PDIA3) plays an important role in influenza infection, inflammation, and airway mechanics. Redox Biology 22, 101129.

14. Chen, K-K, Minakuchi, M, Wuputra, K, Ku, C-C, Pan, J-B, Kuo, K-K, Lin, Y-C, Saito, S, Lin, C-S, and Yokoyama, KK (2020). Redox control in the pathophysiology of influenza virus infection. BMC Microbiology 20, 214.

15. Ciriolo, MR, Palamara, AT, Incerpi, S, Lafavia, E, Buè, MC, Vito, PD, Garaci, E, and Rotilio, G (1997). Loss of GSH, Oxidative Stress, and Decrease of Intracellular pH as Sequential Steps in Viral Infection *. Journal of Biological Chemistry 272, 2700–2708.

16. De Angelis, M, Amatore, D, Checconi, P, Zevini, A, Fraternale, A, Magnani, M, Hiscott, J, De Chiara, G, Palamara, AT, and Nencioni, L (2022). Influenza Virus Down-Modulates G6PD Expression and Activity to Induce Oxidative Stress and Promote Its Replication. Frontiers in Cellular and Infection Microbiology 11.

17. Di Meo, S, Reed, TT, Venditti, P, and Victor, VM (2016). Role of ROS and RNS Sources in Physiological and Pathological Conditions. Oxid Med Cell Longev 2016, 1245049.

18. Dooley, CT, Dore, TM, Hanson, GT, Jackson, WC, Remington, SJ, and Tsien, RY (2004). Imaging Dynamic Redox Changes in Mammalian Cells with Green Fluorescent Protein Indicators *. Journal of Biological Chemistry 279, 22284–22293.

19. Dou, D, Revol, R, Östbye, H, Wang, H, and Daniels, R (2018). Influenza A Virus Cell Entry, Replication, Virion Assembly and Movement. Frontiers in Immunology 9.

20. Eisfeld, AJ, Neumann, G, and Kawaoka, Y (2015). At the centre: influenza A virus ribonucleoproteins. Nat Rev Microbiol 13, 28–41.

21. Ellgaard, L, and Ruddock, LW (2005). The human protein disulphide isomerase family: substrate interactions and functional properties. EMBO Reports 6, 28–32.

22. Flory, E, Kunz, M, Scheller, C, Jassoy, C, Stauber, R, Rapp, UR, and Ludwig, S (2000). Influenza Virus-induced NF-κB-dependent Gene Expression Is Mediated by Overexpression of Viral Proteins and Involves Oxidative Radicals and Activation of IκB Kinase *. Journal of Biological Chemistry 275, 8307–8314.

23. Foo, J, Bellot, G, Pervaiz, S, and Alonso, S (2022). Mitochondria-mediated oxidative stress during viral infection. Trends in Microbiology 30, 679–692.

24. Fukai, T, and Ushio-Fukai, M (2011). Superoxide Dismutases: Role in Redox Signaling, Vascular Function, and Diseases. Antioxid Redox Signal 15, 1583–1606.

25. Gottlieb, RA (2003). Cytochrome P450: major player in reperfusion injury. Arch Biochem Biophys 420, 262–267.

26. Gutscher, M, Pauleau, A-L, Marty, L, Brach, T, Wabnitz, GH, Samstag, Y, Meyer, AJ, and Dick, TP (2008). Real-time imaging of the intracellular glutathione redox potential. Nat Methods 5, 553–559.

27. Hanson, GT, Aggeler, R, Oglesbee, D, Cannon, M, Capaldi, RA, Tsien, RY, and Remington, SJ (2004). Investigating Mitochondrial Redox Potential with Redox-sensitive Green Fluorescent Protein Indicators *. Journal of Biological Chemistry 279, 13044–13053.

28. Huang, Q, Sivaramakrishna, RP, Ludwig, K, Korte, T, Böttcher, C, and Herrmann, A (2003). Early steps of the conformational change of influenza virus hemagglutinin to a fusion active state: stability and energetics of the hemagglutinin. Biochim Biophys Acta 1614, 3–13.

29. Jaulmes, A, Sansilvestri-Morel, P, Rolland-Valognes, G, Bernhardt, F, Gaertner, R, Lockhart, BP, Cordi, A, Wierzbicki, M, Rupin, A, and Verbeuren, TJ (2009). Nox4 mediates the

expression of plasminogen activator inhibitor-1 via p38 MAPK pathway in cultured human endothelial cells. Thrombosis Research 124, 439–446.

30. Jones, DP (2002). Redox potential of GSH/GSSG couple: assay and biological significance. Methods Enzymol 348, 93–112.

31. Kaushal, GP, Chandrashekar, K, and Juncos, LA (2019). Molecular Interactions Between Reactive Oxygen Species and Autophagy in Kidney Disease. International Journal of Molecular Sciences 20, 3791.

32. Khomich, OA, Kochetkov, SN, Bartosch, B, and Ivanov, AV (2018). Redox Biology of Respiratory Viral Infections. Viruses 10, 392.

33. Krammer, F et al. (2018). Influenza. Nat Rev Dis Primers 4, 1–21.

34. Lazrak, A, Iles, KE, Liu, G, Noah, DL, Noah, JW, and Matalon, S (2009). Influenza virus M2 protein inhibits epithelial sodium channels by increasing reactive oxygen species. FASEB J 23, 3829–3842.

35. Lin, X, Wang, R, Zou, W, Sun, X, Liu, X, Zhao, L, Wang, S, and Jin, M (2016). The Influenza Virus H5N1 Infection Can Induce ROS Production for Viral Replication and Host Cell Death in A549 Cells Modulated by Human Cu/Zn Superoxide Dismutase (SOD1) Overexpression. Viruses 8, 13.

36. Lohman, JR, and Remington, SJ (2008). Development of a family of redox-sensitive green fluorescent protein indicators for use in relatively oxidizing subcellular environments. Biochemistry 47, 8678–8688.

37. Meyer, AJ, and Dick, TP (2010). Fluorescent protein-based redox probes. Antioxid Redox Signal 13, 621–650.

38. Mittal, M, Siddiqui, MR, Tran, K, Reddy, SP, and Malik, AB (2014). Reactive Oxygen Species in Inflammation and Tissue Injury. Antioxid Redox Signal 20, 1126–1167.

39. Morgan, B, Sobotta, MC, and Dick, TP (2011). Measuring E(GSH) and H2O2 with roGFP2-based redox probes. Free Radic Biol Med 51, 1943–1951.

40. Mp, M (2009). How mitochondria produce reactive oxygen species. The Biochemical Journal 417.

41. Nayak, DP, Balogun, RA, Yamada, H, Zhou, ZH, and Barman, S (2009). Influenza virus morphogenesis and budding. Virus Res 143, 147–161.

42. Perez, JT, García-Sastre, A, and Manicassamy, B (2013). Insertion of a GFP reporter gene in influenza virus. Curr Protoc Microbiol Chapter 15, 15G.4.1-15G.4.16.

43. Pinto, LH, and Lamb, RA (2006). The M2 proton channels of influenza A and B viruses. J Biol Chem 281, 8997–9000.

44. Pyo, C-W, Shin, N, Jung, KI, Choi, JH, and Choi, S-Y (2014). Alteration of copper–zinc superoxide dismutase 1 expression by influenza A virus is correlated with virus replication. Biochemical and Biophysical Research Communications 450, 711–716.

45. R, M, R, DB, R, V, C, F, and C, G (2005). Novel mechanisms of natural antioxidant compounds in biological systems: involvement of glutathione and glutathione-related enzymes. The Journal of Nutritional Biochemistry 16.

46. Rota, C, Chignell, CF, and Mason, RP (1999). Evidence for free radical formation during the oxidation of 2'-7'-dichlorofluorescin to the fluorescent dye 2'-7'-dichlorofluorescein by horseradish peroxidase: possible implications for oxidative stress measurements. Free Radic Biol Med 27, 873–881.

47. Russell, CJ (2016). Orthomyxoviruses: Structure of Antigens. Reference Module in Biomedical Sciences, B978-0-12-801238-3.95721-0.

48. Samji, T (2009). Influenza A: understanding the viral life cycle. Yale J Biol Med 82, 153–159.

49. Schrader, M, and Fahimi, HD (2004). Mammalian peroxisomes and reactive oxygen species. Histochem Cell Biol 122, 383–393.

50. Sgarbanti, R et al. (2011). Redox Regulation of the Influenza Hemagglutinin Maturation Process: A New Cell-Mediated Strategy for Anti-Influenza Therapy. Antioxidants & Redox Signaling 15, 593–606.

51. Shin, N, Pyo, C-W, Jung, KI, and Choi, S-Y (2015). Influenza A virus PB1-F2 is involved in regulation of cellular redox state in alveolar epithelial cells. Biochem Biophys Res Commun 459, 699–705.

52. Tarpey, MM, Wink, DA, and Grisham, MB (2004). Methods for detection of reactive metabolites of oxygen and nitrogen: in vitro and in vivo considerations. Am J Physiol Regul Integr Comp Physiol 286, R431-444.

53. Taubenberger, JK, and Kash, JC (2010). Influenza virus evolution, host adaptation, and pandemic formation. Cell Host Microbe 7, 440–451.

54. Taubenberger, JK, and Morens, DM (2006). 1918 Influenza: the Mother of All Pandemics. Emerg Infect Dis 12, 15–22.

55. Truong, TH, and Carroll, KS (2013). Redox Regulation of Protein Kinases. Crit Rev Biochem Mol Biol 48, 332–356.

56. Wu, R-F, Ma, Z, Liu, Z, and Terada, LS (2010). Nox4-Derived H2O2 Mediates Endoplasmic Reticulum Signaling through Local Ras Activation. Molecular and Cellular Biology 30, 3553–3568.

57. Yang, H-C, Cheng, M-L, Ho, H-Y, and Tsun-Yee Chiu, D (2011). The microbicidal and cytoregulatory roles of NADPH oxidases. Microbes and Infection 13, 109–120.

58. Zeeshan, HMA, Lee, GH, Kim, H-R, and Chae, H-J (2016). Endoplasmic Reticulum Stress and Associated ROS. International Journal of Molecular Sciences 17, 327.

59. Zuo, L, and Clanton, TL (2002). Detection of reactive oxygen and nitrogen species in tissues using redox-sensitive fluorescent probes. Methods Enzymol 352, 307–325.

60. (2019). Past Pandemics | Pandemic Influenza (Flu) | CDC. Available at: https://www.cdc.gov/flu/pandemic-resources/basics/past-pandemics.html. Accessed March 31, 2023.